HHS Public Access

Author manuscript

Cell Rep. Author manuscript; available in PMC 2024 April 17.

Published in final edited form as:

Cell Rep. 2024 March 26; 43(3): 113942. doi:10.1016/j.celrep.2024.113942.

PAD4 controls tumor immunity via restraining the MHC class II machinery in macrophages

Michael R. Pitter[1,2,3,4], **Ilona Kryczek**[1,2], **Hongjuan Zhang**[1,2], **Nisha Nagarsheth**[1,2], **Houjun Xia**[1,2], **Zhenyu Wu**[1], **Yuzi Tian**[1], **Karolina Okla**[1,2], **Peng Liao**[1,2], **Weichao Wang**[1,2], **Jiajia Zhou**[1,2], **Gaopeng Li**[1,2], **Heng Lin**[1,2], **Linda Vatan**[1,2], **Sara Grove**[1,2], **Shuang Wei**[1,2], **Yongqing Li**[1], **Weiping Zou**[1,2,3,5,6,*]

[1]Department of Surgery, University of Michigan Medical School, Ann Arbor, MI, USA

[2]Center of Excellence for Cancer Immunology and Immunotherapy, Rogel Cancer Center, University of Michigan, Ann Arbor, MI, USA

[3]Department of Pathology, University of Michigan Medical School, Ann Arbor, MI, USA

[4]Graduate Program in Molecular and Cellular Pathology, University of Michigan Medical School, Ann Arbor, MI, USA

[5]Graduate Programs in Immunology and Cancer Biology, University of Michigan Medical School, Ann Arbor, MI, USA

[6]Lead contact

SUMMARY

Tumor-associated macrophages (TAMs) shape tumor immunity and therapeutic efficacy. However, it is poorly understood whether and how post-translational modifications (PTMs) intrinsically affect the phenotype and function of TAMs. Here, we reveal that peptidylarginine deiminase 4 (PAD4) exhibits the highest expression among common PTM enzymes in TAMs and negatively correlates with the clinical response to immune checkpoint blockade. Genetic and pharmacological inhibition of PAD4 in macrophages prevents tumor progression in tumor-bearing mouse models, accompanied by an increase in macrophage major histocompatibility complex (MHC) class II expression and T cell effector function. Mechanistically, PAD4 citrullinates STAT1 at arginine 121, thereby promoting the interaction between STAT1 and protein inhibitor of activated STAT1 (PIAS1), and the loss of PAD4 abolishes this interaction, ablating the inhibitory role of PIAS1 in the expression of MHC class II machinery in macrophages and enhancing T cell activation. Thus,

*Correspondence: wzou@umich.edu.

AUTHOR CONTRIBUTIONS

Conceptualization, M.R.P., H.Z., N.N., and W.Z.; investigation and experimentation, M.R.P.; methodology, M.R.P., I.K., H.Z., H.X., and H.L.; generation of the *Padi4*$^{-/-}$ mice, Z.W., Y.T., and Y.L.; mouse colony management, S.G. and S.W.; bioinformatics, M.R.P.; help with *in vivo* experiments, K.O., P.L., and W.W.; help with the generation of the mutant STAT1 plasmid, J.Z. and G.L.; cell sorting of *STAT1*$^{-/-}$ clones, L.V.; supervision, I.K., Y.L., and W.Z.; writing – original draft, M.R.P.; writing – review & editing, M.R.P., I.K., and W.Z.

SUPPLEMENTAL INFORMATION

Supplemental information can be found online at https://doi.org/10.1016/j.celrep.2024.113942.

DECLARATION OF INTERESTS

W.Z. has served as a scientific advisor or consultant for Cstone, NextCure, and HanchorBio, Inc.

the PAD4-STAT1-PIAS1 axis is an immune restriction mechanism in macrophages and may serve as a cancer immunotherapy target.

Graphical Abstract

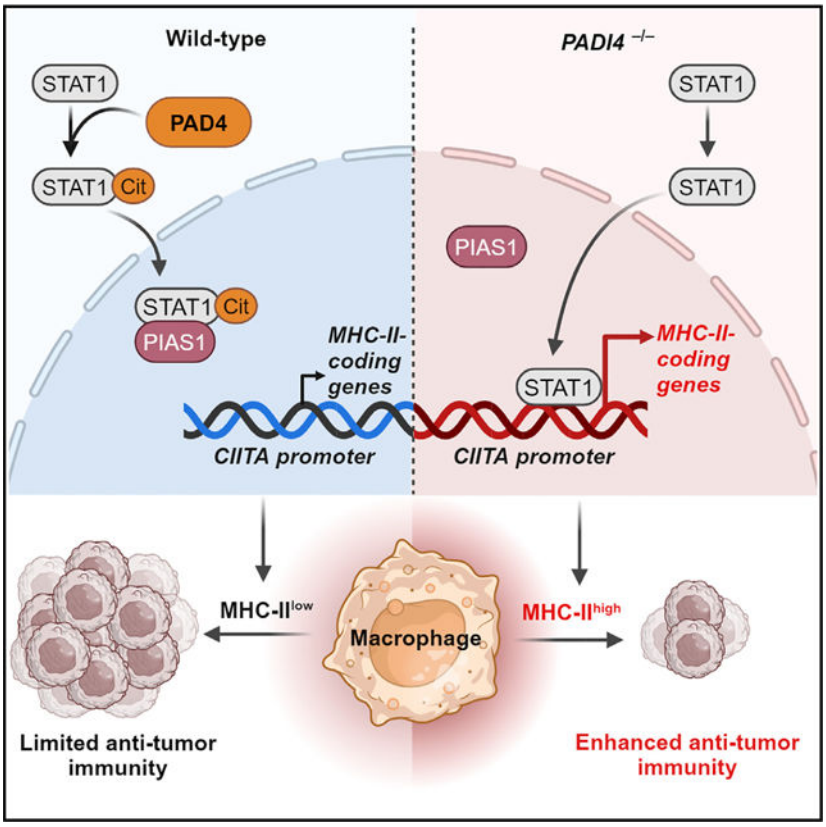

In brief

Pitter et al. demonstrate that the PAD4-mediated citrullination of STAT1 in macrophages enforces the STAT1-PIAS1 interaction restraining STAT1 transcriptional activity and MHC class II machinery expression and, consequently, limits T cell-mediated anti-tumor immunity.

INTRODUCTION

Macrophages are among the major immune cellular components in the tumor microenvironment (TME). Tumor-associated macrophages (TAMs) often markedly outnumber other immune cells, including dendritic cells (DCs), and represent a prominent population of antigen-presenting cells (APCs) in the TME.[1] Previous studies demonstrate high levels of PD-L1 (B7-H1) expression in myeloid APCs, including macrophages and DCs in the human TME and tumor-draining lymph nodes, contributing to immune resistance to immune checkpoint blockade (ICB) in the TME.[2–4] It is generally thought that TAMs play an immunosuppressive role in anti-tumor immune responses.[5–10] Preclinical models show that targeting macrophages, including with anti-CSF1 receptor antibodies, is considered a therapeutic modality.[11–13] However, the number of TAMs can be positively associated with

patient survival in some types of malignancies.[14] Macrophages mediate phagocytosis and present antigens (including tumor antigens) to and activate T cells.[14–16] This apparently paradoxical information has precluded the reaching of a consensus regarding the roles of TAMs and how to target TAMs in human cancer immunotherapy. Furthermore, TAMs are exposed to various environmental factors and would manifest versatile functions depending on the microenvironmental signals, such as metabolites and nutrients.[12,13,17,18] Hence, it is not surprising that directly targeting macrophages has thus far failed to have a major therapeutic impact, although ongoing trials targeting TAMs in combination with other treatment modalities may change the overall picture. It is therefore important to explore previously undocumented intrinsic mechanisms controlling the phenotype and function of macrophages in the TME.

Post-translational modifications (PTMs), including citrullination, are covalent processing events that change the properties of a protein, often resulting in the addition of a modifying group.[19–21] Citrullination is an irreversible PTM catalyzed by peptidyl arginine deiminases (PADs), which convert arginine residues into citrulline.[22] There are 5 active PADs: PAD1–PAD4 and PAD6. It appears that PAD isozymes have mutually exclusive tissue localizations and substrate specificities and citrullinate a wide range of protein substrates and regulate numerous cellular processes, including cell signaling and immune responses.[22–26] Given that PTMs, particularly citrullination, have been extensively studied in cancer cells and neutrophils,[26–29] but not in TAMs, we wondered if PTMs could act as intrinsic mechanism(s) shaping TAM phenotype and function. Therefore, exploration of PTMs in macrophages could generate previously unappreciated insight into TAM immunology. To this end, through cross-analyzing multiple bulk and single-cell RNA sequencing datasets from the mouse and human TMEs, we found that PAD4 manifested the highest expression levels among common PTM enzymes in TAMs and was negatively correlated with clinical response to ICB. Hence, we genetically and biochemically examined the role of PAD4 in determining TAM phenotype and function *in vitro* and *in vivo* in tumor-bearing animal models and assessed the underlying molecular mechanisms. We suggest that targeting PAD4 in TAMs can serve as a potential approach in cancer immunotherapy.

RESULTS

PAD4 is an abundant post-translational-modification enzyme in TAMs

PTMs drive the final conformations and functions of proteins.[30,31] However, it is poorly understood if and how PTMs control TAM functions. To address this question, we analyzed multiple RNA sequencing datasets to assess the expression levels and patterns of major PTM enzymes, including methyltransferases, kinases, ubiquitin enzymes, acyltransferases, acetyltransferases, deacetylases, and peptidylarginine deiminases, in the TAMs of both human and mouse cancers. In patients with breast cancer, differential expression (DE) analysis revealed that PAD4 was the most highly expressed PTM enzyme among major PTM enzymes in TAMs as compared to normal macrophages (Figures 1A, S1A, and 1B).[1] Similar results were obtained in the TAMs of breast-cancer-bearing mice (Figures 1C, S1B, and 1D).[32]

Following the observation that PAD4 expression is enriched in TAMs compared to normal macrophages, we then determined PAD4 expression patterns across immune cell subsets in the TME. We first analyzed a single-cell RNA sequencing dataset featuring $CD45^+$ immune cells from the peritoneal lavage in mice.[33] t-distributed stochastic neighbor embedding (t-SNE)-mediated visualization revealed that *Padi4* was largely expressed in macrophages compared to T cells, B cells, and DCs (Figure 1E). Macrophages contained the highest proportion of *Padi4*-expressing cells (Figure 1F) as well as the highest mRNA expression of *Padi4* (Figure 1G) compared to T cells, B cells, and DCs. In line with the mouse data, analysis of a single-cell RNA sequencing dataset featuring immune cells from patients with colorectal cancer[34] revealed that *PADI4* was also largely expressed in monocytes and macrophages but not in T cells, B cells, or natural killer cells (Figure S1C). Consistent with the mouse data, human macrophages contained the highest proportion of *PADI4*-expressing cells (Figure 1H). Thus, PAD4 is highly enriched in both mouse and human TAMs.

Given the enrichment of PAD4 in TAMs, we asked whether PAD4 expression correlated with an M1- or M2-type TAM phenotype. In patients with triple-negative breast cancer (TNBC),[35] *PADI4* expression correlated with the transcriptional networks known to promote protumor macrophages (Figure S1D). In patients with colorectal cancer,[36] DE analysis revealed that *PADI4* was among the most highly expressed PTM enzyme in $CSF1R^{high}$ TAMs compared to $CSF1R^{low}$ TAMs (Figure S1E). $CSF1R^{high}$ TAMs exhibit a strong immunosuppressive phenotype.[37–39] In ID8 ovarian-cancer-bearing mice, *Padi4* was among the most highly expressed PTM enzymes in peritoneal Tim-4^{high} TAMs as compared to Tim-4^{low} TAMs (Figure S1F). We validated that PAD4 protein was highly expressed in Tim-4^{high} TAMs rather than in Tim-4^{low} TAMs (Figure S1G). Tim-4^{high} TAMs manifest an immunosuppressive phenotype in the TME.[40,41] These data suggest that PAD4 expression correlates with protumor M2-type TAMs. In further support of this possibility, bulk RNA sequencing analysis of TAMs from ID8 tumor-bearing mice showed that the *Padi4*^{high} TAMs expressed lower antigen presentation and T cell activation-associated genes, including *Stat1* and *Ciita* and major histocompatibility complex (MHC) class II-coding genes (Figure S1H). To further support the possibility that PAD4 activity was enhanced in macrophages in the TME, we exposed human primary monocytes and HL60, a myeloid cell line, to ascites fluid from patients with ovarian cancer. We found that ascites fluid increased PAD4 expression in both human primary monocytes and HL60 cells (Figures S1I and S1J). Ovarian cancer ascites fluids contain interleukin-6 (IL-6) and vascular endothelial growth factor (VEGF).[42,43] We showed that both IL-6 and VEGF stimulated PAD4 expression in HL60 cells (Figure S1K). Altogether, these data suggest that PAD4 may be a PTM enzyme driven by tumor microenvironmental factors and that it correlates with the immunosuppressive phenotype of TAMs.

PAD4 in macrophages negatively regulates anti-tumor immunity

To explore a role of PAD4 in macrophages in the context of tumor immune responses, we inoculated subcutaneously MC38 cells, a murine colon adenocarcinoma cell line, into wild-type (*Padi4*$^{+/+}$) and total-body *Padi4* knockout (*Padi4*$^{-/-}$) mice. We found that *Padi4*$^{-/-}$ mice developed smaller tumors compared to *Padi4*$^{+/+}$ mice as shown by tumor volume and weight (Figures 2A, 2B, and S2A). Fluorescence-activated cell sorting analysis (Figure

S2B) revealed that the *Padi4*$^{-/-}$ mice harbored higher levels of interferon γ^{+} (IFNγ^{+}) and interleukin-2^{+} (IL-2^{+}) T cells in the TME as compared to wild-type mice (Figures 2C and 2D). We next asked whether the activated T cell phenotype and reduced tumor progression observed in the *Padi4*$^{-/-}$ tumor-bearing mice were attributed to the loss of PAD4 activity in T cells or macrophages. To specifically examine a role of PAD4 in T cells and macrophages, we bred *Padi4*$^{fl/fl}$ mice with *Cd4*^{cre} and *LysM*^{cre} mice to generate two conditional knockout mouse strains: *Padi4*$^{fl/fl}$ *Cd4*^{cre} (Figure S2C) and *Padi4*$^{fl/fl}$ *LysM*^{cre} mice (Figure S2D). We first asked whether specific loss of PAD4 in T cells could alter anti-tumor immunity in tumor-bearing mice. When we inoculated MC38 cells subcutaneously into *Padi4*$^{fl/fl}$ mice and *Padi4*$^{fl/fl}$ *Cd4*^{cre} mice, we observed no difference in tumor volume and weight (Figure S2E). Interestingly, when we inoculated MC38 cells into *Padi4*$^{fl/fl}$ vs. *Padi4*$^{fl/fl}$ *LysM*^{cre} mice, we observed that the *Padi4*$^{fl/fl}$ *LysM*^{cre} mice developed smaller tumors compared to the wild-type *Padi4*$^{fl/fl}$ counterparts (Figures 2E and 2F). In line with this, there were higher percentages of IFNγ^{+} and tumor necrosis factor alpha^{+} (TNFα^{+})IFNγ^{+} T cells in MC38 tumors (Figures 2G–2J) and higher levels of IFNγ^{+} and TNFα^{+}CD8^{+} T cells in MC38 tumor-draining lymph nodes (Figure S2F) in *Padi4*$^{fl/fl}$ *LysM*^{cre} mice compared to the wild-type mice. Next, using an enzyme-linked immunosorbent spot assay, we detected higher amounts of tumor-specific IFNγ^{+} T cells in MC38 tumors in *Padi4*$^{fl/fl}$ *LysM*^{cre} mice compared to wild-type mice (Figure 2K). Thus, the specific loss of PAD4 in macrophages enhances T cell activation and—consequently—enhances systemic antitumor immunity. To further substantiate this conclusion, we inoculated subcutaneously Py8119 cells, a mouse breast cancer cell line, into *Padi4*$^{fl/fl}$ mice and *Padi4*$^{fl/fl}$ *LysM*^{cre} mice. Again, the *Padi4*$^{fl/fl}$ *LysM*^{cre} mice developed smaller tumors compared to their wild-type counterparts (Figures 2L, 2M, and S2G). To test whether PAD4 deficiency could affect tumor metastasis, we inoculated intravenously B16F10, a murine melanoma cell line, into *Padi*4$^{fl/fl}$ mice and *Padi4*$^{fl/fl}$ *LysM*^{cre} mice. We observed less lung tumor nodules in the *Padi4*$^{fl/fl}$ *LysM*^{cre} mice compared to wild-type counterparts (Figure 2N). We further assessed the T cell activation phenotype in B16F10 lung metastatic nodules in the wild-type and the *Padi4*$^{fl/fl}$ *LysM*^{cre} mice. We observed higher levels of IFNγ- (Figures 2O and 2P) and TNFα-(Figures 2Q and 2R) expressing T cells in the TME of the *Padi4*$^{fl/fl}$ *LysM*^{cre} mice as compared to wild-type mice. Altogether, we conclude that PAD4 in macrophages negatively regulates anti-tumor immunity, thereby promoting tumor progression.

PAD4 restrains MHC class II machinery in macrophages

We next assessed the mechanism by which PAD4 negatively regulates TAM-mediated anti-tumor immunity. First, we compared the immune phenotype of peritoneal macrophages from wild-type and *Padi4*$^{-/-}$ mice. By gating on CD45^{+}CD11b^{+}F4/80^{+} macrophages (Figure S3A), we observed that the levels of MHC class II were higher in *Padi4*$^{-/-}$ macrophages than in *Padi4*$^{+/+}$ macrophages in the peritoneal cavity and lung tissues (Figures 3A–3C and S3B). Interestingly, there was no difference in MHC class I, CD80, and CD86 expression between *Padi4*$^{-/-}$ and *Padi4*$^{+/+}$ macrophages (Figure S3B). We next compared the expression of MHC class II-coding genes as well as the IFNγ signaling gene pathway. We found that the *Padi4*-deficient macrophages expressed higher levels of MHC class II-coding genes, including *H2-Aa*, *Ciita*, and *Cd74*, as well as IFN-signaling genes such as *Stat1* and *Gbp2* (Figure 3D). To validate these findings, we analyzed a publicly available

single-cell RNA sequencing dataset featuring mouse peritoneal immune cells.[33] Based on *Padi4* expression, we divided macrophages into two groups: high *Padi4*- (*Padi4*^{high}) and low *Padi4*- (*Padi4*^{low}) expressing cells (Figure S3C). We found higher expression levels of genes that directly code for MHC class II—such as *H2-Aa*, *H2-Ab1*, and *Ciita*—as well as genes that code for the several co-factors involved in the transcriptional regulation of MHC class II machinery in *Padi4*^{low} macrophages as compared to the *Padi4*^{high} macrophages (Figure S3D). We extended our analysis to TAMs in mice bearing different tumor types, including MC38 and Py8119 subcutaneous tumors and B16 lung metastatic melanoma. Based on previous reports,[44–46] we used the lymphatic vessel endothelial hyaluronan receptor (Lyve1) to identify tissue-resident macrophages in subcutaneous tumor models (Figure S3F). We identified alveolar and interstitial macrophage subsets as tissue-resident and non-tissue-resident macrophages, respectively, in the B16F10 lung metastasis model (Figure S3G).[45,47,48] Flow cytometry analysis revealed an increase in MHC class II expression at different levels in the different *Padi4*$^{fl/fl}$ *LysM*^{cre} macrophage subsets as compared to wild-type macrophages across tumor models (Figures 3E–3G). Thus, PAD4 negatively regulates MHC class II expression on different macrophage subsets via transcriptional regulation.

We validated the inverse relationship between PAD4 and MHC class II-associated signaling in macrophages. Gene set enriched analysis (GSEA) performed on the single-cell RNA sequencing data discussed above revealed that mouse *Padi4*^{high} macrophages manifested several upregulated pathways, including peptidyl-arginine modification (GO: 0018195), protein citrullination (GO: 0018101), and protein-arginine deiminase activity (GO: 0004668), and several downregulated pathways, including antigen processing and presentation of exogenous peptide antigen via MHC class II (GO: 0019886), MHC class II protein complex (GO: 0042613), and IFNγ signaling genes (GO: 0071346) (Figure 3H). Similar results were obtained in human *Padi4*^{high} monocytes (Figure 3H).[49] These GSEA results support our findings that PAD4 negatively regulates MHC class II-associated pathways. Finally, we tested the immune function of enhanced MHC class II in *Padi4*$^{-/-}$ macrophages. To this end, we primed wild-type or *Padi4*$^{-/-}$ macrophages with irradiated ovalbumin-expressing (OVA^{+}) MC38 cells in a co-culture system with OT-II cells.[50] We observed that *Padi4*$^{-/-}$ macrophages induced a higher proportion of IFNγ^{+}CD4^{+} T cells and IL-2^{+}CD4^{+} T cells than *Padi4*$^{+/+}$ macrophages (Figures 3I and 3J). The data suggest that PAD4 restrains MHC class II machinery in macrophages, thereby impairing the antigen-presentation-mediated immune response.

PAD4 citrullinates STAT1 in the N-terminal domain

We next explored how PAD4 could regulate MHC class II expression in macrophages. In response to IFNγ, STAT1 binds to the promoter regions of the class II transactivator (*CIITA*) gene, resulting in the transcription and translation of CIITA, which then mediates the expression MHC class II.[51,52] Moreover, PADs have been shown to be able to regulate transcription factors. For example, PAD2 in T cells regulates transcription factor activity via direct protein citrullination.[53] We hypothesized that PAD4 may directly citrullinate STAT1, thereby regulating STAT1 transcriptional activity and consequently MHC class II expression. To begin to test this hypothesis, we performed the binding analysis for regulation of transcription (BART) on the *Padi4*^{high} mouse peritoneal macrophages.[33] The

BART analysis revealed that STAT1 was one of the most enriched transcription factors that correlated with high expression of PAD4 in mouse macrophages (Figure S4A).[54] It has also been shown that PAD4 directly citrullinates RELA, regulating its transcription factor functions.[55] This observation prompted us to explore a potential regulatory relationship between PAD4 and STAT1. We next tested if PAD4 mediated the citrullination of STAT1. Using a biotin-phenylglyoxal-based chemical probe that specifically modifies peptidyl citrulline under acidic conditions, enabling the visualization of citrullinated proteins,[56] we found that STAT1—in mouse splenocytes (Figures S4B and SAC) and in HL60 (human myeloid leukemia) cells (Figures S4D and S4E)—was citrullinated in response to lipopolysaccharide (LPS) and IFN**γ**. Next, the co-immunoprecipitation (coIP) experiments demonstrated a physical interaction between PAD4 and STAT1 in the *Padi4*$^{+/+}$ mouse macrophages but not in the *Padi4*$^{-/-}$ mouse macrophages (Figure 4A). Furthermore, we detected potent STAT1 citrullination in *Padi4*$^{+/+}$ mouse macrophages, but not *Padi4*$^{-/-}$ mouse macrophages, in response to IFN**γ** (Figure 4B). We validated that the citrullination of STAT1 in response to IFN**γ** and LPS was dependent on PAD4 (Figures 4C and 4D). Moreover, treatment with GSK484, a PAD4-specific inhibitor, suppressed STAT1 citrullination in IFN**γ**-treated HL60 cells (Figure 4E). In an *in vitro* citrullination assay using recombinant proteins, we observed an accumulation of STAT1 citrullination over time in the presence of PAD4 (Figure 4F). Thus, PAD4 mediates the citrullination of STAT1.

We next examined the potential citrullination sites on STAT1. STAT1 includes the N-terminal domain (N-domain), the “coiled-coil” domain, the DNA-binding domain, the linker domain, the SH2 domain, and the C-terminal transactivation domain (Figure S4F). The N-domain is indispensable in the process of STAT1 transcriptional activity.[57–60] PTMs on the N-domain regulate STAT1 transcriptional activity.[21,61] Given these insights, we asked whether the citrullination of STAT1 occurred at the N-domain, which is located within the first 136 amino acids of STAT1 (Figure S4F). To test this possibility, we incubated recombinant STAT1 with recombinant PAD4 protein and then performed mass spectrometry (MS). We found that arginine 121 (R121) was the only residue citrullinated in the N-domain (Figures 4G and 4H). Firstly, the citrullinated form of the peptide ILENAQRNQAQS, containing R121, was identified (Figures 4G and 4H). Interrogation of the high-resolution MS1 spectra confirmed the presence of the 0.98-Da-heavier citrullinated species for this peptide (Figure 4G). The lack of the corresponding monoisotopic peak for the non-citrullinated peptide within the isotopic envelope (indicated by the *m/z* of the far left peak) indicated that citrullination occurred within this peptide (Figure 4G). Generation of the high-resolution MS2 fragmentation spectra localized the site of citrullination to R121. Observation of unmodified ions up to y_{14} demonstrated that the Asn and Gln were not deamidated, a non-enzymatic modification that can also produce a 0.98 Da shift (Figure 4H). The presence of the unmodified b_6 and the modified b_7 ions further validated the citrullinated site, R121 (Figures 4H, 4I, and S4G). In addition, we used the Protein Prospector software[62] to predict the *m/z* values at the b_6 and b_7 ions corresponding to Q120 and R121, respectively, of the ILENAQRNQAQS peptide. The results generated by the software matched our experimental results. Experimentally, through MS, the modified b_7 ions (which correspond to R121) held an *m/z* of 826.43 because of citrullination (Figure 4H). When comparing the *m/z* of R121 in the ILENAQRNQAQS peptide with and without

citrullination using Protein Prospector, the results showed that citrullination induced a shift in *m/z* from 825.45 to 826.43, which precisely matched our experimental results (Figures 4H and 4I). As aforementioned, the b_6 ions were not modified; therefore, with or without citrullination, Q120 sustained the same *m/z* value (Figures 4H and S4G). This peptide residue sequence containing R121—"AQRFN"—is evolutionarily conserved across species (Figure S4H). Altogether, PAD4 directly citrullinates STAT1 at R121 in the N-domain.

STAT1 citrullination facilitates the STAT1-PIAS1 interaction and MHC class II reduction

We next explored if and how PAD4-mediated STAT1 citrullination negatively regulates the transcription of MHC class II-coding genes. Loss of PAD4 enhanced STAT1 signaling and—as a consequence—enhanced MHC class II expression and function (Figure 3). Hence, we hypothesized that STAT1 citrullination resulted in the inhibition of STAT1 transcriptional activity. PIAS1 (protein inhibitor of activated STAT1) physically interacts with STAT1 and, consequently, antagonizes STAT1 DNA binding in the nucleus, thereby resulting in the inhibition of STAT1 transcriptional activity.[63–65] Among the PAD family members, PAD4 is the only isozyme to contain the canonical nuclear localization signal. Thus, we examined the relationship between PAD4 and the STAT1-PIAS1 interaction. To this end, we generated bone-marrow-derived *Padi4*$^{+/+}$ and *Padi4*$^{-/-}$ macrophages and performed a coIP experiment with anti-PIAS1 and probed with anti-STAT1. We detected a potent physical interaction between PIAS1 and STAT1 in *Padi4*$^{+/+}$ macrophages (Figure 5A). Interestingly, the loss of PAD4 largely reduced STAT1 citrullination and abolished the interaction between STAT1 and PIAS1 (Figure 5A). We obtained similar results in freshly isolated peritoneal macrophages from *Padi4*$^{+/+}$ and *Padi4*$^{-/-}$ mice (Figure 5B). We treated HL60 cells with GSK484, a PAD4-specific inhibitor. We detected a potent interaction between STAT1 and PIAS1 in the control conditions; however, treatment with GSK484 reduced this interaction in response to LPS (Figure 5C) and IFNγ (Figure 5D). Thus, PAD4 is required for the interaction between STAT1 and PIAS1.

We next assessed whether the citrullination of STAT1 at R121 was essential for the STAT1-PIAS1 interaction. We used CRISPR-Cas9 to generate *STAT1*$^{-/-}$ HEK293T cells. We ectopically expressed in *STAT1*$^{-/-}$ HEK293T cells a wild-type STAT1 plasmid or a mutated STAT1 plasmid whereby R121 was converted to a lysine (K121). We found that the STAT1 R121K mutants failed to interact with PIAS1, indicating that R121 is essential for the interaction between STAT1 and PIAS1 (Figure 5E). Moreover, we detected an increase in human leukocyte antigen - DR isotype (HLA-DR) expression in cells expressing R121K mutants as compared to cells expressing wild-type STAT1 (Figure 5E). Thus, loss of the STAT1-PIAS1 interaction results in enhanced MHC class II expression. To corroborate the observation that the STAT1-PIAS1 interaction controls MHC class II transcription, we analyzed a publicly available microarray dataset featuring wild-type (*Pias1*$^{+/+}$) vs. *Pias1* knockout (*Pias1*$^{-/-}$) bone-marrow-derived macrophages from mice.[66] We observed higher levels of MHC class II-coding gene (*H2-Aa* and *H2-Ab1*) expression in *Pias1*$^{-/-}$ macrophages compared to *Pias1*$^{+/+}$ macrophages (Figure S5A). The data provide additional evidence that the STAT1-PIAS1 interaction controls MHC class II expression in macrophages.

PIAS1 interacts with STAT1 and antagonizes STAT1 DNA binding.[63,67,68] Therefore, we hypothesized that the loss of the STAT1-PIAS1 interaction resulted in enhanced STAT1 binding to the *CIITA* gene, leading to potentiated MHC class II expression. To test this hypothesis, we performed chromatin immunoprecipitation (ChIP) qPCR to detect STAT1 binding in the *CIITA* gene. ChIP-PCR revealed higher levels of STAT1 occupancies at the key regulatory regions in the *CIITA* gene of *Padi4*$^{-/-}$ mouse cells as compared to *Padi4*$^{+/+}$ mouse cells (Figures S5B and 5F). These regions included *Promoter I*, the classic region for macrophage-specific STAT1 binding in *CIITA*[69,70]; *Peak A* (−47 bp *CIITA*), a recently defined enhancer region in macrophages (Figure S5C)[71]; and exon 2, another critical regulatory region in *CIITA*.[71,72] In line with the mouse data, treatment with GSK484 enhanced STAT1 binding to the *Promoter IV* of *CIITA* in HL60 cells (Figure S5D). *Promoter IV* is an IFNγ-responsive promoter region in human *CIITA*.[69,70,73–75] To demonstrate that PAD4-mediated HLA-DR regulation is PIAS1 dependent, we knocked down PIAS1 using short hairpin RNA in 293T cells. We found that GSK484-mediated PAD4 inhibition failed to enhance HLA-DR expression in response to IFNγ in the absence of PIAS1 (Figure S5E). Together, these data show that STAT1 citrullination facilitates the STAT1-PIAS1 interaction, antagonizing the transcription of MHC class II in macrophages.

PAD4 negatively correlates with IFNγ signaling and impairs therapeutic response to ICB

Finally, we evaluated the therapeutic significance of PAD4 expression in TAMs from patients with cancer and TAMs from tumor-bearing animal models. We first demonstrated that the pharmacological inhibition of PAD4 with GSK484 could upregulate HLA-DR protein in the primary TAMs harvested from patients with ovarian cancer and in human blood monocytes in response to IFNγ (Figures 6A and 6B). We then analyzed a single-cell RNA sequencing dataset featuring immune cells in patients with TNBC receiving ICB therapy.[35] Based on *PADI4* expression in TAMs, we found that the levels of *CIITA* and *HLA-DRA* were higher in *PADI4*^{low} TAMs compared to *PADI4*^{high} TAMs (Figure 6C). In further support of this inverse relationship between HLA-DR-associated genes and *PADI4*, we found a negative correlation between *PADI4* expression and an antigen presentation gene signature in the TAMs of patients with TNBC (Figure S6A). We then analyzed the relationship between PAD4 expression and T cell activation in patients with TNBC. GSEA revealed that *PADI4*^{high} macrophages exhibited an upregulation of citrullination-associated pathways and a downregulation of pathways associated with IFNγ signaling, MHC class II-mediated antigen presentation, and T cell activation (Figure S6B). Analogously, high expression of *PADI4* in TAMs negatively correlated with the response to IFNγ (GO: 0034341) and MHC class II-mediated antigen presentation pathways (GO: 0002495) (Figure 6D). Furthermore, *PADI4* in TAMs negatively correlated with *TBX21* and *IL12RB2* (Figure 6E) expression in CD4^{+} T cells. We next sought to assess the effect of macrophage PAD4 on the response to ICB. Based on clinical response in the single-cell RNA sequencing dataset,[35] we divided the patients into two groups: responders and non-responders (Figure S6C). As expected, TAMs expressed higher levels of *CIITA* (Figure S6D), *HLA-DRA*, and *HLA-DRB1* (Figure S6E) in the responders compared to the non-responders. Importantly, *PADI4* expression in TAMs was higher in the non-responders compared to the responders (Figures 6F and S6F). Finally, we tested the role of PAD4 in the therapeutic response to ICB in MC38-tumor-bearing mouse model. We showed that treatment with GSK484 inhibited

tumor progression and enhanced therapeutic efficacy of PD-L1 blockade in MC38-bearing mice (Figure 6G). Thus, PAD4 plays a negative role in tumor immunity.

DISCUSSION

In this study, we report that PAD4-mediated citrullination in TAMs restrains anti-tumor immunity via antagonizing the IFNγ/STAT1-MHC class II signaling pathway.

TAMs represent a prominent population of APCs in the TME. To discover previously undocumented immune regulatory molecule(s) in TAMs, we have explored the potential involvement of PTMs in the TME. By analyzing multiple sequencing datasets featuring human and mouse immune cells in the TME, we found that among the most common PTM enzymes, *PADI4* (or *Padi4*) was highly enriched in TAMs. *PADI4* expression negatively correlated with the gene signatures of IFNγ and T cell immune responses and with clinical response to ICB. Using several tumor-bearing mouse models with targeted deletion of *Padi4* from macrophages, we demonstrate that PAD4 in macrophages restrains T cell-mediated anti-tumor immunity. Previous studies have largely focused on the role of the PAD-mediated citrullination of histones in the formation of neutrophil extracellular traps[76–79] in autoimmune diseases.[80–82] Our work demonstrates that PAD4 in macrophages plays a previously unrecognized role in negatively regulating anti-cancer immunity. Thus, our study fills the knowledge gap of PAD4 in the field of immunology.

After defining the role for PAD4 in macrophages, we have explored the molecular targets of PAD4 in TAMs. We show that the genetic and pharmacological inhibition of PAD4 results in an increase in several molecules in the MHC class II machinery, particularly MHC class II. This regulation manifests a relative specificity at the cellular and molecular levels. PAD4 expression is highly enriched in TAMs, but not other mononuclear immune cells, in the TME. PAD4 deficiency in macrophages, but not in T cells, has an impact on tumor progression. Thus, it is plausible that PAD4 plays a major role in macrophages rather than other immune cells. Furthermore, *Padi4* deficiency results in the upregulation of MHC class II, but not CD80, CD86, or MHC class I, gene expression in TAMs.

We have studied how PAD4 affects MHC class II expression in macrophages. STAT1 mediates transcriptional regulation of MHC class II.[52] We speculate that PAD4 mediates STAT1 citrullination, thereby altering MHC class II expression in TAMs. Indeed, we show that PAD4 citrullinates STAT1, resulting in reduced MHC class II expression and function. Interestingly, STAT1 citrullination promotes the interaction between STAT1 and PIAS1 in macrophages. Previous studies have defined an inhibitory role of PIAS in the JAK/STAT signaling pathway in macrophages and cancer cells.[66,67,83] PIAS1 is an E3 small ubiquitin-like modifier (SUMO) ligase and can suppress STAT1 transcriptional activity via SUMOylation at lysine 114 (K114) in the N-domain as well as at other regions, leading to dephosphorylation and dissociation of STAT1 from DNA.[67,84–87] PIAS1 can also diminish STAT1 activity via recruiting other transcriptional repressors.[88] We demonstrate that the interaction between PIAS1 and STAT1 depends on STAT1 citrullination. The citrullination of R121 is essential for the STAT1-PAS1 interaction, which negatively regulates MHC class II expression. Thus, loss of PAD4 enhances STAT1 binding to key IFNγ-responsive

promoter regions in the *CIITA* gene, resulting in increased MHC class II transcriptional expression in macrophages and enhanced anti-tumor immunity.

PAD-mediated histone citrullination results in the formation of neutrophil extracellular traps,[76] supporting cancer progression.[78,89] PAD4-mediated STAT1 citrullination impairs TAM-induced tumor immunity. Thus, targeting citrullination in macrophages and neutrophils may constitute a potentially robust immunotherapeutic approach to treating patients with cancer.

Limitations of the study

We show that PAD4 citrullinates STAT1 and controls the STAT1-PIAS1 interaction, thereby altering STAT1 transcriptional activity and MHC class II expression. Given that PIAS1 is a SUMO ligase, it remains to be studied whether PIAS1 SUMOylation affects the PAD4-regulated STAT1 activity. Previous studies on the role of PAD4 hypercitrullination in promoting rheumatoid arthritis have shown that specific mutations in the *PADI4* gene drive the enhanced citrullination activity. Such study would add additional information on how to target PAD4 in macrophages for cancer treatment. Moreover, further work is needed to elucidate why the PAD4-STAT1-PIAS1 axis selectively targets MHC class II and whether this axis regulates other downstream molecular targets.

STAR⋆METHODS

RESOURCE AVAILABILITY

Lead contact—Further information and requests for resources and reagents should be directed to and will be fulfilled by the lead contact, Weiping Zou (wzou@umich.edu).

Materials availability—No reagents were generated in the study.

Data and code availability

- The original mass spectrometry proteomics data have been deposited to the ProteomeXchange Consortium via the PRIDE partner repository and are publicly available as of the date of publication. The accession number is listed in the key resources table.
- This paper does not report original code.
- This paper analyzes existing, publicly available bulk and single-cell RNA sequencing data. These accession numbers for the datasets are listed in the key resources table.

EXPERIMENTAL MODEL AND SUBJECT PARTICIPANT DETAILS

Cell lines—HL60 cells (CCL-240), HEK293T cells (CRL-3216), B16F10 (CRL-6475) and Py8119 (CRL-3278) were purchased from the American Type Culture Collection (ATCC, Manassas, VA). Use of the MC38 cells were previously reported.[3] HEK293T, MC38, B16F10 and Py8119 cells were maintained in RPMI-1640 Medium (HyClone SH30255, GE Healthcare, Chicago, IL) supplemented with 10% fetal bovine serum. HL60 cells were

maintained in Iscove's modified Dulbecco's medium (IMDM) supplemented with 20% fetal bovine serum. All cell lines were tested for *Mycoplasma* contamination by MycoAlert Mycoplasma Detection Kit and confirmed negative for *Mycoplasma*. All cells were cultured at 37°C under a humidified atmosphere containing 5% CO_2.

Animal models—*Padi4*$^{fl/fl}$ mice, *LysM*^{cre} mice, *Cd4*^{cre} mice, and wild type C57BL/6J mice were purchased from the Jackson Laboratory. *Padi4*$^{-/-}$ mice were generated in house (Yongqing Li). *Padi4*$^{fl/fl}$ mice were crossed with *LysM*^{cre} mice to generate both wild-type *Padi4*$^{+/+}$ *LysM*^{cre} mice and *Padi4*$^{fl/fl}$ *LysM*^{cre} mice, which are deficient in their macrophage expression of *Padi4*. Respectively, these mice are referred to as *Padi4*$^{fl/fl}$ (*LysM*^{Cre}+) and *Padi4*$^{fl/fl}$ *LysM*^{cre} (*LysM*^{Cre}–). *Padi4*$^{fl/fl}$ mice were crossed with *Cd4*^{cre} mice to generate both wild-type *Padi4*$^{+/+}$ *Cd4*^{cre} and *Padi4*$^{fl/fl}$ *Cd4*^{cre} mice, which are deficient in their CD4$^+$ and CD8$^+$ T cell expression of *Padi4*. As above, these mice are referred to as *Padi4*$^{fl/fl}$ (*Cd4*^{Cre}+) and *Padi4*$^{fl/fl}$ *Cd4*^{cre} (*Cd4*^{Cre}–). Mice were bred in the specific-pathogen-free animal facility (~22°C with ~40% humidity) on a 12 h dark/12 h light cycle at the University of Michigan. All procedures were approved by the Institutional Animal Care and Use Committees (IACUC) and the Unit for Laboratory Animal Medicine (ULAM) at the University of Michigan.

Murine colon carcinoma (MC38) cells (3×10^6) were injected subcutaneously into the left flanks of age- and sex-matched *Padi4*$^{-/-}$ or C57BL/6J mice (8–10 weeks); *Padi4*$^{+/+}$ *Cd4*^{cre} or *Padi4*$^{fl/fl}$ *Cd4*^{cre} mice (8–10 weeks) and *Padi4*$^{+/+}$ *LysM*^{cre} or *Padi4*$^{fl/fl}$ *LysM*^{cre} mice (8–10 weeks). Py8119 breast adenocarcinoma cells (2×10^4) were injected subcutaneously into the left flanks of age-matched, female *Padi4*$^{+/+}$ *LysM*^{cre} or *Padi4*$^{fl/fl}$ *LysM*^{cre} mice (8–10 weeks). Tumor monitoring began 7 days after inoculation and continued every 3 days until endpoint. Tumor length, width and height was measured with calipers fitted with a Vernier scale. Tumor volume was calculated as previously described90. B16F10 murine melanoma (2×10^5) was injected intravenously into the tail vein of age- and sex-matched *Padi4*$^{+/+}$ *LysM*^{cre} or *Padi4*$^{fl/fl}$ *LysM*^{cre} mice (8–10 weeks).

Anti-PD-L1 and IgG1 isotype antibodies were given intraperitoneally at a dose of 100 μg per mouse on day 7 after tumor cell inoculation and then every 3 days for the duration of the experiment. Mice received 3 doses total. GSK484 was administered intraperitoneally at a dose of 4 mg/kg per mouse as previously described[96] every day for the duration of the experiment.

Human samples—Primary ascites fluid was collected from patients with ovarian cancer at the University of Michigan and used as an agonist to induce PAD4 expression in HL60 cells or in primary human monocytes. The study for which we acquired the patient ascites fluid was approved by the Institutional Review Boards of the University of Michigan (IRB: HUM00054493). Human monocytes were positively enriched from blood buffy coats (Carter BloodCare) using the EasySep Human Monocyte Isolation Kit (STEMCELL Technologies). Monocytes were differentiated into macrophages following overnight stimulation with 1 μg/mL LPS and 10 ng/mL IFNγ. Patient mononuclear cells from primary patient ovarian tumors (Cooperative Human Tissue Network) were isolated from the tumor mass following processing into a single-cell suspension and then submitting to Ficoll density gradient

centrifugation. Mononuclear cells were then cultured in RPMI-1640 medium supplemented with 10% fetal bovine serum. TAMs were then identified via fluorescent staining as $CD45^+CD14^+$ mononuclear cells and analyzed via FACS. All human samples in our studies were collected with informed consent from each individual donor.

METHOD DETAILS

Magnetic-activated cell sorting (MACS) of peritoneal macrophages—Mice were euthanized via a CO_2 overdose and peritoneal lavage was harvested in MACS buffer on ice. 10–15 mL of peritoneal lavage per mouse was collected after multiple washes of the peritoneal cavity. Cell suspensions were centrifuged and resuspended to be incubated with the primary PE–anti–Tim-4 antibody (clone RMT4–54, BD Biosciences) diluted (1:10) in MACS buffer at 4°C for 10 min in the dark. Cells were washed and centrifuged. The supernatant was aspirated completely and the pellet was resuspended in 80μL of MACS buffer prior to adding and mixing 20μL of anti–PE microbeads (Miltenyi Biotec) for a 15-min incubation at 4°C in the dark. Cells were washed, centrifuged and resuspended in MACS buffer. The PE positive cells were sorted by passing them through LS columns (Miltenyi) according to the manufacturer's instructions. Enriched macrophages were cultured in Dulbecco's Modified Eagle Medium (DMEM) supplemented with 10% fetal bovine serum. The purity of the enriched PE positive cells ranged between 86 and 91% across experiments.

Generation of mouse bone marrow–derived macrophages—Mice were euthanized via a CO_2 overdose and the tibias and femurs were removed and scraped to isolate the bones only. Marrow was flushed out of the bones into a Petri dish with DMEM supplemented with 10% fetal bovine serum and 100X penicillin-streptomycin. Bone marrow cells were plated at 5×10^6 per well in 6 well plates and then treated with 10 ng/mL M-CSF. On Day 3 after plating, half of the volume of media per well was removed and replaced with fresh media. Cells were treated again with 10 ng/mL M-CSF. On Day 6, cells were treated with 2 μg/mL LPS and/or 10 ng/mL IFNγ to complete maturation.

Isolation of primary mouse splenocytes—Mice were euthanized via a CO_2 overdose and spleens were removed. Spleens were mashed with a 1 mL syringe plunger and washed through a 70μM strainer over a 50 μL conical tube to collect 35 mL of a single-cell suspension. To isolate splenocytes from the granulocytes and other splenic tissue cells, we remove the latter subsets via density gradient centrifuge by overlaying the 35 mL of single-cell suspension on top of 15 mL of 100% Ficoll. After centrifugation, with a reduced-speed starting and ending, the enriched layer of splenocytes was visible. The layer was removed and washed. Cells were quantified prior to experimentation.

Isolation of primary T-cells from OT-II transgenic mice—Mice were euthanized via a CO_2 overdose and spleens were removed. Primary splenocytes were isolated in the process described above. Lymphocytes also served as a source for T-cells. Lymph nodes were removed from the euthanized mice and smashed with a 1 mL syringe plunger and washed through a 70μM strainer over a 50 μL conical tube to collect 35 mL of a single-cell suspension containing splenocytes and/or lymphocytes. T-cells were isolated from the

splenocyte and/or lymphocyte single–cell suspensions using EasySep Mouse $CD3^+$ T cell Isolation Kit (STEMCELL Technologies).

***In vitro* antigen presentation–mediated OT-II T cell activation assay—**OT-II cells from the OT-II transgenic mice were isolated as described above. T-cells were either cultured alone, co-cultured with *Padi4*$^{+/+}$ or *Padi4*$^{-/-}$ macrophages, or co-cultured with the macrophages and with ovalbumin–expressing (OVA^+) MC38 cells (OVA, Sigma Aldrich) in RPMI-1640 medium supplemented with 10% fetal bovine serum. Tumor cells were first osmotically loaded with 10 mg/mL ovalbumin and then irradiated with ultraviolet (UV) light in 10 mm dishes as previously described.[97] 2×10^5 T-cells from OT-II transgenic mice were culture alone, or co-cultured only with 1×10^4 peritoneal macrophages, or with macrophages and 1×10^5 dead tumor cells in flat 96 well plates. After a 4-day incubation period in 37°C under a humidified atmosphere containing 5% CO_2, cells were harvested and activated T cell cytokine production was assessed via fluorescent staining and FACS analysis.

***In vitro* citrullination assay—**Recombinant human PAD4 (Sigma-Aldrich) was incubated with recombinant human STAT1 (Abcam) in a buffer containing 100mM HEPES, 2mM $CaCl_2$ and water at 37°C.

Detection of citrullination—Cells were lysed with 0.2% SDS and further disrupted with sonication. Protein lysates were then incubated with phenylglyoxal-biotin (PG-biotin) (0.1mM) in a buffer containing 50mM HEPES and 20% trichloroacetic acid at 37°C for 30-min as previously described.[56] Biotin-PG-labeled citrullinated proteins were then captured with streptavidin-agarose beads (Thermo Fisher) overnight at 4°C. The captured proteins were then subjected to Western blotting.

Identification of citrullination site by LC-Tandem MS

In-gel digestion: The protein samples were processed and analyzed at the Mass Spectrometry Facility of the Department of Pathology at the University of Michigan. Gel slice corresponding human STAT1 was destained with 30% methanol for 4 h. Upon reduction (10 mM DTT) and alklylation (65 mM 2-Chloroacetamide) of the cysteines, proteins were digested overnight with 500 ng of sequencing grade, modified trypsin (Promega) at 37°C. Peptides were extracted by incubating the gel with 150 μL of 50% acetonitrile/0.1% TFA for 30 min at room temperature. A second extraction with 150 μL of 100% acetonitrile/0.1% TFA was also performed. Both extracts were combined and dried in a vacufuge (Eppendorf).

Mass spectrometry: Resulting peptides were dissolved in 9 μL of 0.1% formic acid/2% acetonitrile solution. Two μLs of the resulting peptide solution were resolved on a nano-capillary reverse phase column (Acclaim PepMap C18, 2 μm, 50 cm, ThermoScientific) using a 0.1% formic acid/acetonitrile gradient at 300 nL/min over a period of 90 min (2–25% acetonitrile in 35 min; 25–50% acetonitrile in 20 min followed by a 90% acetonitrile wash for 5 min and a further 30 min re-equilibration with 2% acetonitrile). Eluent was directly introduced into *Q Exactive HF* mass spectrometer (Thermo Scientific, San Jose

CA) using an EasySpray source. MS1 scans were acquired at 60K resolution (AGC target = 3×10^6; max IT = 50 ms). Data-dependent collision induced dissociation MS/MS spectra were acquired on 20 most abundant ions following each MS1 scan (NCE ~28%; AGC target 1×10^5; max IT 45 ms).

Database search: Proteins were identified by searching the data against the UniProt human protein database (20315 entries; downloaded on 01/05/2023) using Proteome Discoverer (v2.4, Thermo Scientific). Search parameters included MS1 mass tolerance of 10 ppm and fragment tolerance of 0.05 Da; two missed cleavages were allowed; carbamidomethylation of cysteine (+57.012 Da) was considered fixed modification and oxidation of methionine (+15.994 Da), deamidation of arginine, asparagine and glutamine (+0.984 Da), were considered as potential modifications. False discovery rate (FDR) was determined using Percolator and proteins/peptides with an FDR of ≤1% were retained for further analysis.

Flow cytometry analysis—Single-cell suspensions were prepared from fresh mouse peritoneal lavage, lungs, spleen, lymph nodes, and tumor tissues. For surface staining alone, single cell suspensions were washed with PBS, pelleted via centrifugation and then resuspended in 50 μL of MACS buffer. Fluorescent antibodies were added and a 20-min incubation followed at room temperature protected from light. For intracellular cytokine staining, lymphocytes were incubated in culture medium containing phorbol 12-myristate-13-acetate (5 ng mL^{-1}; Sigma-Aldrich), ionomycin (500 ng mL^{-1}; Sigma-Aldrich), brefeldin A (1:1000; BD Biosciences) and monensin (1:1000; BD Biosciences) at 37°C for 4 h. Antibodies (0.6 μg) were added for 20-min for surface staining. The cells were then washed and resuspended in 1 mL freshly prepared Fix/Perm solution (BD Biosciences) at 4°C overnight. After being washed with Perm/Wash buffer (BD Biosciences), the cells were staining with 0.6 μg antibodies against intracellular proteins from 30-min, washed and fixed in 4% formaldehyde (Sigma-Aldrich). All samples were read on an LSR II cytometer and analyzed with FACS DIVA software v. 8.0 (BD Biosciences).

IFNγ ELISpot assay—Multiscreen filtration plates (96-wells/plate; Mabtech) were pre-coated with anti-mouse interferon-γ (IFNγ) monoclonal antibody (clone AN18; Mabtech). T-cells were enriched from the tumors of wild-type and $Padi4^{fl/fl}$ $LysM^{cre}$ MC38–bearing mice. Tumor T-cells were added (1×10^5 cells/well) and stimulated for 20 h with UV-irradiated mouse MC38 cells (5×10^4 cells/well). Bonded IFNγ was detected by biotinylated rat anti-mouse IFNγ monoclonal antibody (R4–6A2; Mabtech) followed by anti-biotin streptavidin alkaline phosphatase. Spots were developed and visualized with 5-bromo-4-chloro-3-indolyl phosphate (BCIP)/nitro blue tetrazolium (NBT)–plus substrate and counted using a Luminex 200 Instrument System (Thermo Fisher). Results were quantified by calculating the ratio of the number of ELI spots detected to the number of T-cells plated per well.

Immunoblotting—Protein was extracted from the cells with RIPA buffer supplemented with 100X protease inhibitor (Thermo) and resolved on SDS-PAGE gels, then transferred to nitrocellulose or PVDF membranes. The primary antibodies against mouse PADI4 (1:1000, Abcam, ab214810), STAT1 (1:1000, CST, 9172), phosphor-STAT1 (Tyr107)

(1:1000, CST, 9167), PIAS1 (1:1000, CST, 3350), β-actin (1:1000, CST, 3700), MHC-II (1:1000, Abcam, ab55152 or ab180779), CIITA (1:500, Abcam, ab70060) and HLA-DR (1:1000, Abcam, ab118347) were used. Peroxidase-conjugated secondary antibody (Vector Laboratories) was used and the antigen-antibody reaction was visualized using an enhanced chemiluminescence assay (ECL, BioRad).

Co-immunoprecipitation (Co-IP)—The cells were prepared in IP lysis buffer with 100X protease inhibitor (Thermo Fisher Scientific) and further disrupted by repeated passage through a 21-gauge needle and sonication. Lysates were then centrifuged for 15 min at 12,000rpm and 4°C. Next, for pre-clearance, the supernatants were incubated with Protein A/G plus-agarose (SCBT) and with the IgG isotype control antibody for 30 min in rotation at 4°C. Samples were then incubated with indicated antibodies (2μg/sample) overnight at 4°C followed by a 4-h incubation with Protein A/G plus-agarose at 4°C.

Quantitative PCR analysis—Total RNA was isolated from cells by column purification (Direct-zol RNA Miniprep kit; Zymo Research) with DNase treatment. Complementary DNA (cDNA) was synthesized using a High-Capacity cDNA Reverse Transcription Kit (Thermo Fisher Scientific) with poly-dT or random hexamer primers. Quantitative PCR was performed on cDNA using Fast SYBR Green Master Mix (Thermo Fisher Scientific) on a QuantStudio 3 Real-Time PCR System (Thermo Fisher Scientific). Gene expression was quantified using the following primers:

mouse *H2-Aa* forward: GGAGGTGAAGACGACATTGAGG

mouse *H2-Aa* reverse: CTCAGGAAGCATCCAGACAGTC

mouse *Cd74* forward: GCTGGATGAAGCAGTGGCTCTT

mouse *Cd74* reverse: GATGTGGCTGACTTCTTCCTGG

mouse *Ciita* forward: ACCTTCGTCAGACTGGCGTTGA

mouse *Ciita* reverse: GCCATTGTATCACTCAAGGAGGC

mouse *Stat1* forward: GCCTCTCATTGTCACCGAAGAAC

mouse *Stat1* reverse: TGGCTGACGTTGGAGATCACCA

mouse *Gbp2* forward: ACCAAGGGCATCTGGATGTG

mouse *Gbp2* reverse: TAGCGGAATCGTCTACCCCA

mouse β-actin forward: AGATCAAGATCATTGCTCCTCCT

mouse β-actin reverse: ACGCAGCTCAGTAACAGTCC.

Chromatin immunoprecipitation (ChIP) quantitative PCR analysis—ChIP assay was performed according to the SimpleChIP Enzymatic Chromatin IP Kit (CST, 9003). In brief, cells were fixed with formaldehyde and lysed, and chromatin was fragmented by partial digestion with Micrococcal Nuclease to obtain chromatin fragments of 1–5 nucleosomes. ChIP was performed using antibodies against STAT1 (CST, 9172) and IgG control (CST, 2729), and ChIP-Grade Protein G Magnetic

Beads. After reversal of protein–DNA cross-links, the DNA was purified using DNA purification spin columns, ChIP–enriched chromatin was used for real-time PCR. Relative expression levels were normalized to input. Immunoprecipitation of STAT1 on the *Ciita* (mouse) or *CIITA* (human) gene was quantified using the following primers: mouse *promoter I* (forward: CTGCACCGGAATGAGGAAAC; reverse: AGCCTTGCAGCATCCAAAAC); mouse *peak A* (forward: GGTGGTGACATCG CTGTATGAC; reverse: TCTCCTCCACACAGGCTTGAG); mouse *exon 2* (forward: AGAGGGCAGCTACCTGGAACTC; reverse: GCCA GGTCCATCTGGTCATAG); human *promoter IV* (forward: TCACGGTTGGACTGAGTTGG; reverse: CCTGAGTTGCAGGGAGCTTG). STAT1 DNA binding was quantified using the Fold enrichment method (also known as signal over background). ChIP signals are divided by the non-antibody signals, representing the ChIP signal as the fold increase in signal relative to the background signal. The cycle threshold (CT) value detected from the mock IgG sample is subtracted from the CT value detected from the antibody sample to compute the ΔΔCT value. Fold enrichment is calculated by computing the $2^{-(\Delta\Delta CT)}$ value from the antibody samples.

Generation of mutant plasmids—STAT1 mutant plasmids were generated to form a single nucleotide mutation converting R121 into K121 in the STAT1 protein. The Site–Directed Mutagenesis Kit (200523) was used to generate the PCR product containing the STAT1-R121K mutant sequence. The mutant PCR product was then transformed using XL-1 Blue super compentant cells and then selected for kanamycin resistance on agar. Plasmids were then purified using the QIAprep Spin Miniprep Kit (QIAGEN). The mutant plasmids used for the overexpression of human mutant STAT1 (forward: CGCCCAGAAATTTAATCAGGCTCAGTCGGGGAA; reverse: TTAAATTTCTGGGCGTTTTCCAG AATTTTCCT) were generated.

Transfection of HEK-293T cells—Transfection of HEK-293T cells with the mutant STAT1R121K plasmid was performed using the Lipofectamine 2000 (ThermoFisher) kit. HEK 293T cells were seeded at 1×10^6 cells per well in a 6-well plate. After 24 h, the Lipofectamine reagent and the mutant STAT1-R121K plasmid were diluted separately in Opti-MEM Medium. The diluted Lipofectamine reagent and the diluted mutant STAT1 plasmid were then applied to the cultured cells to be transfected. Cells were analyzed 1–3 days later. All transfections were conducted at a ratio of 1μg plasmid: 2μL transfection reagent.

Bioinformatic analysis—Bulk and single-cell RNA-seq counts were obtained from the Gene Expression Omnibus database with the accession numbers GSE117970, GSE212643, GSE193814, GSE157673, GSE146771, GSE121521, GSE165905, GSE1552 and GSE169246. In our analysis of bulk RNA sequencing data, raw counts were processed and normalized using Limma-Voom tools. Quality control measures were performed, raw counts were transformed into log counts per million and trimmed mean of M values (TMM) normalization methods were applied prior to assessing gene expression levels between groups. Differential expression analysis was performed using the EdgeR package. Single-cell RNA-seq data were processed and analyzed using the Seurat (v. 4.3.0.1) workflow[90] as

previously described.[17] Immune cell subsets were determined based on the annotations of the clusters computed during the Seurat workflow. Comparisons of TAM gene expression between TNBC patient Responders and Non-responders to ICB therapy were achieved by applying single-cell RNA-seq data integration tools provided by Seurat. tSNE plots were generated using the RunTSNE package with Seurat object inputs. Gene set enrichment analysis (GSEA) was performed using the gseGO package. Generation of the antigen presentation gene set signature (Figure S6A) was achieved using the UCell package. Microarray data were RMA normalized. Prediction of functional relationship between PAD4 expression and transcription factor STAT1 in macrophages was performed by analyzing the *Padi4*^{high} macrophage gene set with binding analysis for regulation of transcription (BART).[54] ProteinProspector v.6.4.9 (UCSF), was used to determine the theoretical mass-to-charge ratio (m/z) of each amino acid within the noncitrullinated versus the citrullinated ILENAQRNQAQS peptide of interest.

QUANTIFICATION AND STATISTICAL ANALYSIS

No statistical methods were used to predetermine sample size. Statistical significance was calculated between two separate groups (i.e., wild-type versus knockout or control versus treatment) by an unpaired two-tailed Student's t test. Statistical significance was calculated between two groups of the same cellular source (i.e., primary patient ovarian cancer TAMs treated with IFNγ subjected to treatment with DMSO or GSK484) by a paired two-tailed Student's t test. The Mann-Whitney *U*-test was applied for comparisons between two separate groups of continuous outcomes. It has been shown that nonparametric tests are suitable for epigenetic data.[98–100] One-Way analysis of variance (ANOVA) was applied to determine statistical difference between multiple (3 or more) experimental groups. Cell-based experiments were performed with at least 3 biological and 3 technical replicates unless otherwise stated. All FACS analysis was performed on at least 3 biological replicates. Animal experiments were performed with C57BL/6 mice including *Padi4*$^{+/+}$, *Padi4*$^{-/-}$, *Padi4*$^{fl/fl}$, *Padi4*$^{fl/fl}$ *LysM*^{cre} and *Padi4*$^{fl/fl}$ *Cd4*^{cre} mice. Wild-type vs. *Padi4*–deficient mice were sex and age-matched during tumor inoculation. At least 5–10 mice were used for each group. Statistical analysis for animal or cell–based experiments was performed using GraphPad Prism9. Statistical analysis within the bioinformatic data was performed using RStudio.

Supplementary Material

Refer to Web version on PubMed Central for supplementary material.

ACKNOWLEDGMENTS

We thank Dr. Venkatesha Basrur at the Mass Spectrometry Facility in the Department of Pathology at the University of Michigan for his guidance on the interpretation of the liquid chromatography-tandem MS results. We thank Dr. Paul Thompson and his laboratory members at the University of Massachusetts Chan Medical School for sharing their relevant research protocols and providing helpful discussion. This work was supported in part by research grants from US NIH/NCI R01 grants (CA217648, CA123088, CA099985, CA193136, and CA152470) and the NIH through the University of Michigan Rogel Cancer Center Grant (CA46592).

REFERENCES

1. Cassetta L, Fragkogianni S, Sims AH, Swierczak A, Forrester LM, Zhang H, Soong DYH, Cotechini T, Anur P, Lin EY, et al. (2019). Human Tumor-Associated Macrophage and Monocyte Transcriptional Landscapes Reveal Cancer-specific Reprogramming, Biomarkers, and Therapeutic Targets. Cancer Cell 35, 588–602.e10. [PubMed: 30930117]
2. Curiel TJ, Wei S, Dong H, Alvarez X, Cheng P, Mottram P, Krzysiek R, Knutson KL, Daniel B, Zimmermann MC, et al. (2003). Blockade of B7-H1 improves myeloid dendritic cell–mediated antitumor immunity. Nat. Med 9, 562–567. [PubMed: 12704383]
3. Lin H, Wei S, Hurt EM, Green MD, Zhao L, Vatan L, Szeliga W, Herbst R, Harms PW, Fecher LA, et al. (2018). Host expression of PD-L1 determines efficacy of PD-L1 pathway blockade-mediated tumor regression. J. Clin. Invest 128, 1708. [PubMed: 29608143]
4. Liu Y, Zugazagoitia J, Ahmed FS, Henick BS, Gettinger SN, Herbst RS, Schalper KA, and Rimm DL (2020). Immune Cell PD-L1 Colocalizes with Macrophages and Is Associated with Outcome in PD-1 Pathway Blockade Therapy. Clin. Cancer Res 26, 970–977. [PubMed: 31615933]
5. Mills CD, Kincaid K, Alt JM, Heilman MJ, and Hill AM (2000). M-1/M-2 macrophages and the Th1/Th2 paradigm. J. Immunol 164, 6166–6173. [PubMed: 10843666]
6. Sinha P, Clements VK, and Ostrand-Rosenberg S (2005). Reduction of myeloid-derived suppressor cells and induction of M1 macrophages facilitate the rejection of established metastatic disease. J. Immunol 174, 636–645. [PubMed: 15634881]
7. Rodriguez PC, Zea AH, DeSalvo J, Culotta KS, Zabaleta J, Quiceno DG, Ochoa JB, and Ochoa AC (2003). L-arginine consumption by macrophages modulates the expression of CD3 zeta chain in T lymphocytes. J. Immunol 171, 1232–1239. [PubMed: 12874210]
8. Pollard JW (2004). Tumour-educated macrophages promote tumour progression and metastasis. Nat. Rev. Cancer 4, 71–78. [PubMed: 14708027]
9. Wyckoff J, Wang W, Lin EY, Wang Y, Pixley F, Stanley ER, Graf T, Pollard JW, Segall J, and Condeelis J (2004). A paracrine loop between tumor cells and macrophages is required for tumor cell migration in mammary tumors. Cancer Res. 64, 7022–7029. [PubMed: 15466195]
10. Sanford DE, Belt BA, Panni RZ, Mayer A, Deshpande AD, Carpenter D, Mitchem JB, Plambeck-Suess SM, Worley LA, Goetz BD, et al. (2013). Inflammatory Monocyte Mobilization Decreases Patient Survival in Pancreatic Cancer: A Role for Targeting the CCL2/CCR2 Axis. Clin. Cancer Res 19, 3404–3415. [PubMed: 23653148]
11. Zhu Y, Knolhoff BL, Meyer MA, Nywening TM, West BL, Luo J, Wang-Gillam A, Goedegebuure SP, Linehan DC, and DeNardo DG (2014). CSF1/CSF1R Blockade Reprograms Tumor-Infiltrating Macrophages and Improves Response to T-cell Checkpoint Immunotherapy in Pancreatic Cancer Models. Cancer Res. 74, 5057–5069. [PubMed: 25082815]
12. Vitale I, Manic G, Coussens LM, Kroemer G, and Galluzzi L (2019). Macrophages and Metabolism in the Tumor Microenvironment. Cell Metab. 30, 36–50. [PubMed: 31269428]
13. Mantovani A, Allavena P, Marchesi F, and Garlanda C (2022). Macrophages as tools and targets in cancer therapy. Nat. Rev. Drug Discov 21, 799–820. [PubMed: 35974096]
14. Bingle L, Brown NJ, and Lewis CE (2002). The role of tumour-associated macrophages in tumour progression: implications for new anticancer therapies. J. Pathol 196, 254–265. [PubMed: 11857487]
15. Zavadova E, Loercher A, Verstovsek S, Verschraegen CF, Micksche M, and Freedman RS (1999). The role of macrophages in antitumor defense of patients with ovarian cancer. Hematol. Oncol. Clin. North Am 13, 135–144. [PubMed: 10080073]
16. Ohno S, Suzuki N, Ohno Y, Inagawa H, Soma GI, and Inoue M (2003). Tumor-associated macrophages: foe or accomplice of tumors? Anticancer Res. 23, 4395–4409. [PubMed: 14666727]
17. Li S, Yu J, Huber A, Kryczek I, Wang Z, Jiang L, Li X, Du W, Li G, Wei S, et al. (2022). Metabolism drives macrophage heterogeneity in the tumor microenvironment. Cell Rep. 39, 110609. [PubMed: 35385733]
18. Xia HJ, Wang W, Crespo J, Kryczek I, Li W, Wei S, et al. (2017). Suppression of FIP200 and autophagy by tumor-derived lactate promotes naive T cell apoptosis and affects tumor immunity. Science Immunology 2.

19. Uy R, and Wold F (1977). Posttranslational covalent modification of proteins. Science 198, 890–896. [PubMed: 337487]
20. Walsh CT, Garneau-Tsodikova S, and Gatto GJ (2005). Protein Posttranslational Modifications: The Chemistry of Proteome Diverifications. Angew. Chem. Int. Ed 44, 7342–7372.
21. Mowen KA, and David M (2014). Unconventional post-translational modification in immunological signaling. Nat. Immunol 15, 512–520. [PubMed: 24840982]
22. Yu K, and Proost P (2022). Insights into peptidylarginine deiminase expression and citrullination pathways. Trends Cell Biol. 32, 746–761. [PubMed: 35197210]
23. Thompson PR, and Fast W (2006). Histone Citrullination by Protein Arginine Deiminase: Is Arginine Methylation a Green Light or a Road-block? ACS Chem. Biol 1, 433–441.
24. Christophorou MA, Castelo-Branco G, Halley-Stott RP, Oliveira CS, Loos R, Radzisheuskaya A, Mowen KA, Bertone P, Silva JCR, Zernicka-Goetz M, et al. (2014). Citrullination regulate pluripotency and histone H1 binding to chromatin. Nature 507, 104–108. [PubMed: 24463520]
25. Mondal S, and Thompson PR (2019). Protein Arginine Deiminases (PADs): Biochemistry and Chemical Biology of Protein Citrullination. Acc. Chem. Res 52, 818–832. [PubMed: 30844238]
26. Yuzhalin AE (2019). Citrullination in Cancer. Cancer Res. 79, 1274–1284. [PubMed: 30894374]
27. Wang L, Song G, Zhang X, Feng T, Pan J, Chen W, Yang M, Bai X, Pang Y, Yu J, et al. (2017). PADI2-Mediated Citrullination Promotes Prostate Cancer Progression. Cancer Res. 77, 5755–5768. [PubMed: 28819028]
28. Thålin C, Lundström S, Seignez C, Daleskog M, Lundström A, Henriksson P, Helleday T, Phillipson M, Wallén H, and Demers M (2018). Citrullinated histone H3 as a novel prognostic blood marker in patients with advanced cancer. PLoS One 13, e0191231. [PubMed: 29324871]
29. Moshkovich N, Ochoa HJ, Tang B, Yang HH, Yang Y, Huang J, Lee MP, and Wakefield LM (2020). Peptidylarginine Deiminase IV Regulates Breast Cancer Stem Cells via a Novel Tumor Cell-Autonomous Suppressor Role. Cancer Res. 80, 2125–2137. [PubMed: 32265227]
30. Mann M, and Jensen ON (2003). Proteomic analysis of post-translational modifications. Nat. Biotech 21, 255–261.
31. Deribe YL, Pawson T, and Dikic I (2010). Post-translational modifications in signal integration. Nat. Struct. Mol. Biol 17, 666–672. [PubMed: 20495563]
32. Nixon BG, Kuo F, Ji L, Liu M, Capistrano K, Do M, Franklin RA, Wu X, Kansler ER, Srivastava RM, et al. (2022). Tumor-associated macrophages expressing the transcription factor IRF8 promote T cell exhaustion in cancer. Immunity 55, 2044–2058.e5. [PubMed: 36288724]
33. Wang YT, Zaitsev K, Lu Q, Li S, Schaiff WT, Kim KW, Droit L, Wilen CB, Desai C, Balce DR, et al. (2020). Select autophagy genes maintain quiescence of tissue-resident macrophages and increase susceptibility to *Listeria monocytogenes*. Nat. Microbiol 5, 272–281. [PubMed: 31959973]
34. Zhang L, Li Z, Skrzypczynska KM, Fang Q, Zhang W, O'Brien S, He Y, Wang L, Zhang Q, Kim A, et al. (2020). Single-Cell Analyses Inform Mechanisms of Myeloid-Targeted Therapies in Colon Cancer. Cell 181, 442–459.e29. [PubMed: 32302573]
35. Zhang Y, Chen H, Mo H, Hu X, Gao R, Zhao Y, Liu B, Niu L, Sun X, Yu X, et al. (2021). Single-cell analyses reveal key immune cell subsets associated with response to PD-L1 blockade in triple-negative breast cancer. Cancer Cell 39, 1578–1593.e8. [PubMed: 34653365]
36. Wang X, Zhang J, Hu B, and Qian F (2022). High Expression of CSF-1R Predicts Poor Prognosis and CSF-1Rhigh Tumor-Associated Macrophages Inhibit Anti-Tumor Immunity in Colon Adenocarcinoma. Front. Oncol 12, 850767. [PubMed: 35444953]
37. Pyonteck SM, Akkari L, Schuhmacher AJ, Bowman RL, Sevenich L, Quail DF, Olson OC, Quick ML, Huse JT, Teijeiro V, et al. (2013). CSF-1R inhibition alters macrophage polarization and blocks glioma progression. Nat. Med 19, 1264–1272. [PubMed: 24056773]
38. Tap WD, Wainberg ZA, Anthony SP, Ibrahim PN, Zhang C, Healey JH, Chmielowski B, Staddon AP, Cohn AL, Shapiro GI, et al. (2015). Structure–Guided Blockade of CSF1R Kinase in Tenosynovial Gient-Cell Tumor. N. Engl. J. Med 373, 428–437. [PubMed: 26222558]
39. Candido JB, Morton JP, Bailey P, Campbell AD, Karim SA, Jamieson T, Lapienyte L, Gopinathan A, Clark W, McGhee EJ, et al. (2018). $CSF1R^{+}$ Macrophages Sustain Pancreatic Tumor Growth

through T Cell Suppression and Maintenance of Key Gene Programs that Define the Squamous Subtype. Cell Rep. 23, 1448–1460. [PubMed: 29719257]

40. Xia H, Li S, Li X, Wang W, Bian Y, Wei S, Grove S, Wang W, Vatan L, Liu JR, et al. (2020). Autophagic adaptation to oxidative stress alters peritoneal residential macrophage survival and ovarian cancer metastasis. JCI Insight 5, e141115. [PubMed: 32780724]
41. Chow A, Schad S, Green MD, Hellmann MD, Allaj V, Ceglia N, Zago G, Shah NS, Sharma SK, Mattar M, et al. (2021). Tim-4^{+} cavity-resident macrophages impair anti-tumor CD8^{+} T cell immunity. Cancer Cell 39, 973–988.e9. [PubMed: 34115989]
42. Kryczek I, Lange A, Mottram P, Alvarez X, Cheng P, Hogan M, Moons L, Wei S, Zou L, Machelon V, et al. (2005). CXCL12 and vascular growth factor synergistically induce neoangiogenesis in human ovarian cancer. Cancer Res. 65, 465–472. [PubMed: 15695388]
43. Kryczek I, Zou L, Rodriguez P, Zhu G, Wei S, Mottram P, Brumlik M, Cheng P, Curiel T, Myers L, et al. (2006). B7-H4 expression identifies a novel suppressive macrophage population in human ovarian carcinoma. J. Exp. Med 203, 871–881. [PubMed: 16606666]
44. Lim HY, Lim SY, Tan CK, Thiam CH, Goh CC, Carbajo D, Chew SHS, See P, Chakarov S, Wang XN, et al. (2018). Hyaluronan receptor LYVE-1–expressing macrophages maintain arterial tone through hyaluronan–mediated regulation of smooth muscle cell collagen. Immunity 49, 1191–1341. [PubMed: 30566884]
45. Chakarov S, Lim HY, Tan L, Lim SY, See P, Lum J, Zhang XM, Foo S, Nakamizo S, Duan K, et al. (2019). Two distinct interstitial macrophage populations coexist across tissues in specific subtissular niches. Science 363, eaau0964. [PubMed: 30872492]
46. Dick SA, Wong A, Hamidzada H, Nejat S, Nechanitzky R, Vohra S, Mueller B, Zaman R, Kantores C, Aronoff L, et al. (2022). Three tissue resident macrophage subsets coexist across organs with conserved origins and life cycles. Sci. Immunol 7, eabf7777. [PubMed: 34995099]
47. Hussell T, and Bell TJ (2014). Alveolar macrophages: plasticity in a tissue–specific context. Nat. Rev. Immunol 14, 81–93. [PubMed: 24445666]
48. Schyns J, Bai Q, Ruscitti C, Radermecker C, De Schepper S, Chakarov S, Farnir F, Pirottin D, Ginhoux F, Boeckxstaens G, et al. (2019). Non-classical tissue monocytes and two functionally distinct population of interstitial macrophages populate the mouse lung. Nat. Commun 10, 3964. [PubMed: 31481690]
49. Wimmers F, Donato M, Kuo A, Ashuach T, Gupta S, Li C, Dvorak M, Foecke MH, Chang SE, Hagan T, et al. (2021). The single-cell epigenomic and transcriptional landscape of immunity to influenza vaccination. Cell 184, 3915–3935.e21. [PubMed: 34174187]
50. Denning TL, Wang YC, Patel SR, Williams IR, and Pulendran B (2007). Lamina propria macrophages and dendritic cells differentially induce regulatory and interleukin 17–producing T cell responses. Nat. Immunol 8, 1086–1094. [PubMed: 17873879]
51. Meraz MA, White JM, Sheehan KC, Bach EA, Rodig SJ, Dighe AS, Kaplan DH, Riley JK, Greenlund AC, Campbell D, et al. (1996). Targeted Disruption of the Stat1 Gene in Mice Reveals Unexpected Physiologic Specificity in the JAK–STAT Signaling Pathway. Cell 84, 431–442. [PubMed: 8608597]
52. Ting JPY, and Trowsdale J (2002). Genetic control of MHC class II expression. Cell 109, S21–S33. [PubMed: 11983150]
53. Sun B, Chang HH, Salinger A, Tomita B, Bawadekar M, Holmes CL, Shelef MA, Weerapana E, Thompson PR, and Ho IC (2019). Reciprocal regulation of Th2 and Th17 cells by PAD2–mediated citrullination. JCI Insight 4, e129687. [PubMed: 31723060]
54. Wang Z, Civelek M, Miller CL, Sheffield NC, Guertin MJ, and Zang C (2018). a transcription factor prediction tool with query gene sets of epigenomic profiles. Bioinformatics 34, 2867–2869. [PubMed: 29608647]
55. Sun B, Dwivedi N, Bechtel TJ, Paulsen JL, Muth A, Bawadekar M, Li G, Thompson PR, Shelef MA, Schiffer CA, et al. (2017). Citrullination of NF-kB p65 promotes its nuclear localization and TLR–induced expression of IL-1β and TNFα. Sci. Immunol 2, eaal3062. [PubMed: 28783661]
56. Bicker KL, Subramanian V, Chumanevich AA, Hofseth LJ, and Thompson PR (2012). Seeing Citrulline: Development of a phenylglyoxal-based probe to visualize protein citrulline. J. Am. Chem. Soc 134, 17015–17018. [PubMed: 23030787]

57. Vinkemeier U, Moarefi I, Darnell JE, and Kuriyan J (1998). Structure of the Amino-Terminal Protein Interaction Domain of STAT-4. Science 279, 1048–1052. [PubMed: 9461439]
58. Ota N, Brett TJ, Murphy TL, Fremont DH, and Murphy KM (2004). N-domain–dependent nonphosphorylated STAT4 dimers required for cytokine-driven activation. Nat. Immunol 5, 208–215. [PubMed: 14704793]
59. Reich NC, and Liu L (2006). Tracking STAT nuclear traffic. Nat. Rev. Immunol 6, 602–612. [PubMed: 16868551]
60. Göder A, Ginter T, Heinzel T, Stroh S, Fahrer J, Henke A, and Krämer OH (2021). STAT1 N-terminal domain discriminatively controls type I and type II IFN signaling. Cytokine 144, 155552. [PubMed: 34000478]
61. Mowen KA, Tang J, Zhu W, Schurter BT, Shuai K, Herschman HR, and David M (2001). Arginine methylation of STAT1 modulates IF-Nalpha/beta–induced transcription. Cell 104, 731–741. [PubMed: 11257227]
62. Baker PR, and Clauser PR. Protein Prospector. 1996–2023. http://prospector.ucsf.edu.
63. Hu X, Li J, Fu M, Zhao X, and Wang W (2021). The JAK/STAT signaling pathway: from bench to clinic. Signal Transduct. Target. Ther 6, 402. [PubMed: 34824210]
64. ten Hoeve J, de Jesus Ibarra-Sanchez M, Fu Y, Zhu W, Tremblay M, David M, and Shuai K (2002). Identification of a nuclear Stat1 protein tyrosine phosphatase. Mol. Cell Biol 22, 5662–5668. [PubMed: 12138178]
65. Croker BA, Kiu H, and Nicholson SE (2008). SOCS Regulation of the JAK/STAT Signaling Pathway. Semin. Cell Dev. Biol 19, 414–422. [PubMed: 18708154]
66. Liu B, Mink S, Wong KA, Stein N, Getman C, Dempsey PW, Wu H, and Shuai K (2004). PIAS1 selectively inhibits interferon–inducible genes and is important in innate immunity. Nat. Immunol 5, 891–898. [PubMed: 15311277]
67. Liu B, Liao J, Rao X, Kushner SA, Chung CD, Chang DD, and Shuai K (1998). Inhibition of Stat1-mediated gene activation by PIAS1. Proc. Natl. Acad. Sci. USA 95, 10626–10631. [PubMed: 9724754]
68. Shuai K, and Liu B (2005). Regulation of Gene-activation pathways by PIAS proteins in the immune system. Nat. Rev. Immunol 5, 593–605. [PubMed: 16056253]
69. Waldburger JM, Suter T, Fontana A, Acha-Orbea H, and Reith W (2001). Selective Abrogation of Major Histocompatibility Complex Class II Expression on Extrahematopoietic Cells in Mice Lacking Promoter IV of the Class II Transactivator Gene. J. Exp. Med 194, 393–406. [PubMed: 11514597]
70. Reith W, LeibundGut-Landmann S, and Waldburger JM (2005). Regulation of MHC Class II Gene Expression by the Class II Transactivator. Nat. Rev. Immunol 5, 793–806. [PubMed: 16200082]
71. Buxadé M, Encado HH, Riera-Borrull, Quintana-Gallardo L, López-Cotarelo, Tellechea M, et al. (2018). Macrophage–specific MHCII expression is regulated by a remote *Ciita* enhancer controlled by NFAT5. J. Exp. Med 215, 2901–2918. [PubMed: 30327417]
72. Muhlethaler-Mottet A, Otten LA, Steimle V, and Mach B (1997). Expression of MHC class II molecules in different cellular and functional compartments is controlled by differential usage of multiple promoters of the transactivator CIITA. EMBO J. 16, 2851–2860. [PubMed: 9184229]
73. Ni Z, Abou El Hassan M, Xu Z, Yu T, and Bremner R (2008). The chromatin-remodeling enzyme BRG1 coordinates *CIITA* induction through many interdependent distal enhancers. Nat. Immunol 9, 785–793. [PubMed: 18500344]
74. Muhlethaler-Mottet A, Di Berardino W, Otten LA, and Mach B (1998). Activation of the MHC Class II Transactivator CIITA by Interferon-g Requires Cooperative Interaction between Stat1 and USF-1. Immunity 8, 157–166. [PubMed: 9491997]
75. Ni Z, Karaskov E, Yu T, Callaghan SM, Der S, Park DS, Xu Z, Pattenden SG, and Bremner R (2005). Apical role for BRG1 in cytokine-induced promoter assembly. Proc. Natl. Acad. Sci. USA 102, 14611–14616. [PubMed: 16195385]
76. Li P, Li M, Lindberg MR, Kennett MJ, Xiong N, and Wang Y (2010). PAD4 is essential for antibacterial innate immunity mediated by neutrophil extracellular traps. JEM 207, 1853–1862.

77. Albrengues J, Shields MA, Ng D, Park CG, Ambrico A, Poin-dexter ME, Upadhyay P, Uyeminami DL, Pommier A, Küttner V, et al. (2018). Neutrophil extracellular traps produced during inflammation awaken dormant cancer cells in mice. Science 361, eaao4227. [PubMed: 30262472]
78. Yang L, Liu Q, Zhang X, Liu X, Zhou B, Chen J, Huang D, Li J, Li H, Chen F, et al. (2020). DNA of neutrophil extracellular traps promotes cancer metastasis via CCDC25. Nature 583, 133–138. [PubMed: 32528174]
79. Munir H, Jones JO, Janowitz T, Hoffmann M, Euler M, Martins CP, Welsh SJ, and Shields JD (2021). Stromal-driven and Amyloidβ–dependent induction of neutrophil extracellular traps modulates tumor growth. Nat. Commun 12, 683. [PubMed: 33514748]
80. Papayannopoulos V (2018). Neutrophil extracellular traps in immunity and disease. Nat. Rev. Immunol 18, 134–147. [PubMed: 28990587]
81. Tilvawala R, Nguyen SH, Maurais AJ, Nemmara VV, Nagar M, Salinger AJ, Nagpal S, Weerapana E, and Thompson PR (2018). The rheumatoid arthritis–associated citrullinome. Cell Chem. Biol 25, 691–704.e6. [PubMed: 29628436]
82. Curran AM, Naik P, Giles JT, and Darrah E (2020). PAD enzymes in rheumatoid arthritis: pathogenic effectors and autoimmune targets. Nat Revs Rheum 16, 301–315.
83. Ungureanu D, Vanhatupa S, Kotaja N, Yang J, Aittomaki S, Jänne OA, Palvimo JJ, and Silvennoinen O (2003). PIAS proteins promote SUMO-1 conjugation to STAT1. Blood 102, 3311–3313. [PubMed: 12855578]
84. Rogers RS, Horvath CM, and Matunis MJ (2003). SUMO Modification of STAT1 and Its Role in PIAS–mediated Inhibition of Gene Activation. J. Biol. Chem 278, 30091–30097. [PubMed: 12764129]
85. Heppler LN, and Frank DA (2017). Targeting Oncogenic Transcription Factors: Therapeutic Implications of Endogenous STAT Inhibitors. Trends Cancer 3, 816–827. [PubMed: 29198438]
86. Begitt A, Meyer T, van Rossum M, and Vinkemeier U (2000). Nucleocytoplasmic translocation of Stat1 is regulated by a leucine-rich export signal in the coiled-coil domain. Proc. Natl. Acad. Sci. USA 97, 10418–10423. [PubMed: 10973496]
87. Haspel RL, and Darnell JE (1999). A nuclear protein tyrosine phosphatase is required for the inactivation of Stat1. Proc. Natl. Acad. Sci. USA 96, 10188–10193. [PubMed: 10468584]
88. Li C, McManus FP, Plutoni C, Pascariu CM, Nelson T, Alberici Delsin LE, Emery G, and Thibault P (2020). Quantitative SUMO proteomics identifies PIAS1 substrates involved in cell migration and motility. Nat. Commun 11, 834. [PubMed: 32047143]
89. Deng H, Lin C, Garcia-Gerique L, Fu S, Cruz Z, Bonner EE, Rosenwasser M, Rajagopal S, Sadhu MN, Gajendran C, et al. (2022). A novel selective inhibitor JBI-589 targets PAD4–mediated neutrophil migration to suppress tumor progression. Cancer Res. 82, 3561–3572. [PubMed: 36069973]
90. Satija R, Farrell JA, Gennert D, Schier AF, and Regev A (2015). Spatial reconstruction of single-cell gene expression data. Nat. Biotechnol 33, 495–502. [PubMed: 25867923]
91. Yu G, Wang L, Han Y, and He Q (2012). clusterProfiler: an R package for comparing biological themes among gene clusters. OMICS. A Journal of Integrative Biology 16, 284–287. [PubMed: 22455463]
92. McInnes L, Healy J, Saul N, and Grobberger L (2018). UMAP: Uniform Manifold Approximation and Projection. Journal of Open Source Software 3, 861.
93. Kuleshov MV, Jones MR, Rouillard AD, Fernandez NF, Duan Q, Wang Z, Koplev S, Jenkins SL, Jagodnik KM, et al. (2016). Enrichr: a comprehensive gene set enrichment analysis web server 2016 update. Nucleic Acids Res 44. W90–7. [PubMed: 27141961]
94. Wickham H (2016). ggplot2: Elegant graphics for data analysis (New York: Springer-Verlag).
95. Wickham H, FranÇois R, Henry L, MÜller K, and Vaughan D (2023). dplyr: A grammar of data manipulation. https://dplyr.tidyverse.org, https://github.com/tidyverse/dplyr.
96. Cedervall J, Dragomir A, Saupe F, Zhang Y, Ärnlöv J, Larsson E, Dimberg A, Larsson A, and Olsson AK (2017). Pharmacological targeting of peptidylarginine deminase 4 prevents cancer–associated kidney injury in mice. OncoImmunology 6, e1320009. [PubMed: 28919990]

97. Lin H, Kryczek I, Li S, Green MD, Ali A, Hamasha R, Wei S, Vatan L, Szeliga W, Grove S, et al. (2021). Stanniocalcin 1 is a phagocytosis checkpoint driving tumor immune resistance. Cancer Cell 39, 480–493.e6. [PubMed: 33513345]

98. Rebollo R, Horard B, Begeot F, Delattre M, Gilson E, and Vieira C (2012). A Snapshot of Histone Modifications within Transposable Elements in *Drosophila* Wild Type Strains. PLoS One 7, e44253. [PubMed: 22962605]

99. Popadin K, Gutierrez-Arcelus M, Dermitzakis ET, and Antonarakis SE (2013). Genetic and Epigenetic Regulation of Human lincRNA Gene Expression. AJHG 93, 1015–1026. [PubMed: 24268656]

100. Wang R, Lee JH, Kim J, Xiong F, Hasani LA, Shi Y, Simpson EN, Zhu X, Chen YT, Shivshankar P, et al. (2023). SARS-CoV-2 restructures host chromatin architecture. Nat. Microbiol 8, 679–694. [PubMed: 36959507]

Highlights

- PAD4 is among the most active PTM enzymes in TAMs
- Loss of PAD4 enhances MHC class II and anti-tumor immunity
- PAD4 citrullinates STAT1, facilitating the STAT1-PIAS1 interaction
- STAT1 citrullination negatively correlates with IFNγ signaling and response to ICB

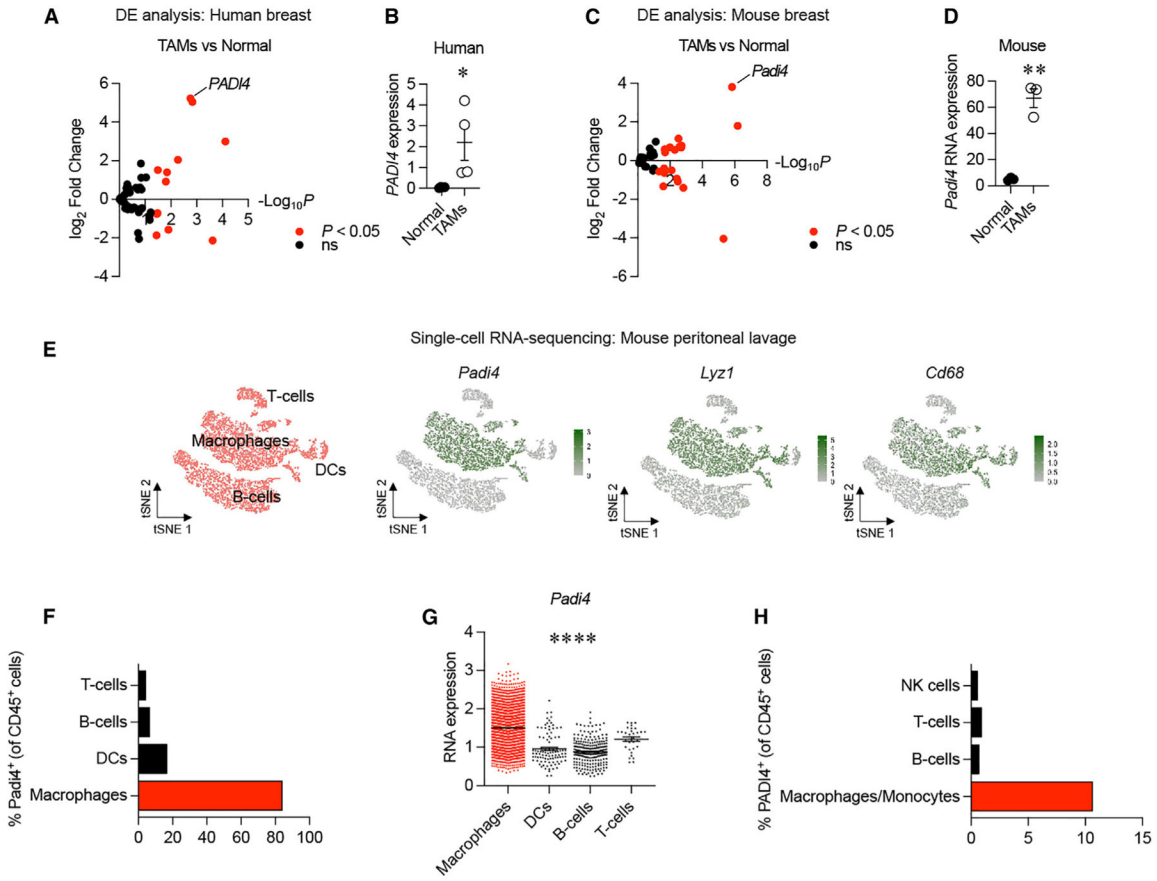

Figure 1. PAD4 is an abundant post-translational modification (PTM) enzyme in TAMs

(A) Differential expression analysis of PTM enzymes in TAMs vs. normal macrophages from patients with breast cancer (GEO: GSE117970).

(B) Human *PADI4* mRNA expression in normal breast macrophages vs. in breast cancer TAMs examined in a bulk RNA sequencing (RNA-seq) dataset (GEO: GSE117970) (n = 4).

(C) Differential expression analysis of PTM enzymes in TAMs vs. normal macrophages from breast-tumor-bearing mice (GEO: GSE212643).

(D) Mouse *Padi4* mRNA expression in normal breast macrophages vs. in breast cancer TAMs examined in a bulk RNA-seq dataset (GEO: GSE212643) (n = 3).

(E) t-Distributed stochastic neighbor embedding (tSNE) plots generated from scRNA-seq data (GEO: GSE121521) showing distribution of macrophage-associated genes across peritoneal lavage subsets from mice.

(F) Proportion of *Padi4*$^{+}$ cells in each immune cell subset of the mouse peritoneal lavage (GEO: GSE121521).

(G) Expression levels of *Padi4* across immune cell subsets of the mouse peritoneal lavage (GEO: GSE121521).

(H) Proportion of *PADI4*$^{+}$ cells in each immune cell subset of peripheral blood mononuclear cells from peripheral blood mononuclear cells (PBMCs) from patients with colorectal cancer (GEO: GSE146771).

Data are shown as mean ± SEM (B, D, and G). Unpaired two-tailed student's t test (B and D). One-way ANOVA test (G). *p < 0.05, **p < 0.01, and ****p < 0.0001. scRNA-seq, single-cell RNA sequencing; ns, not significant.

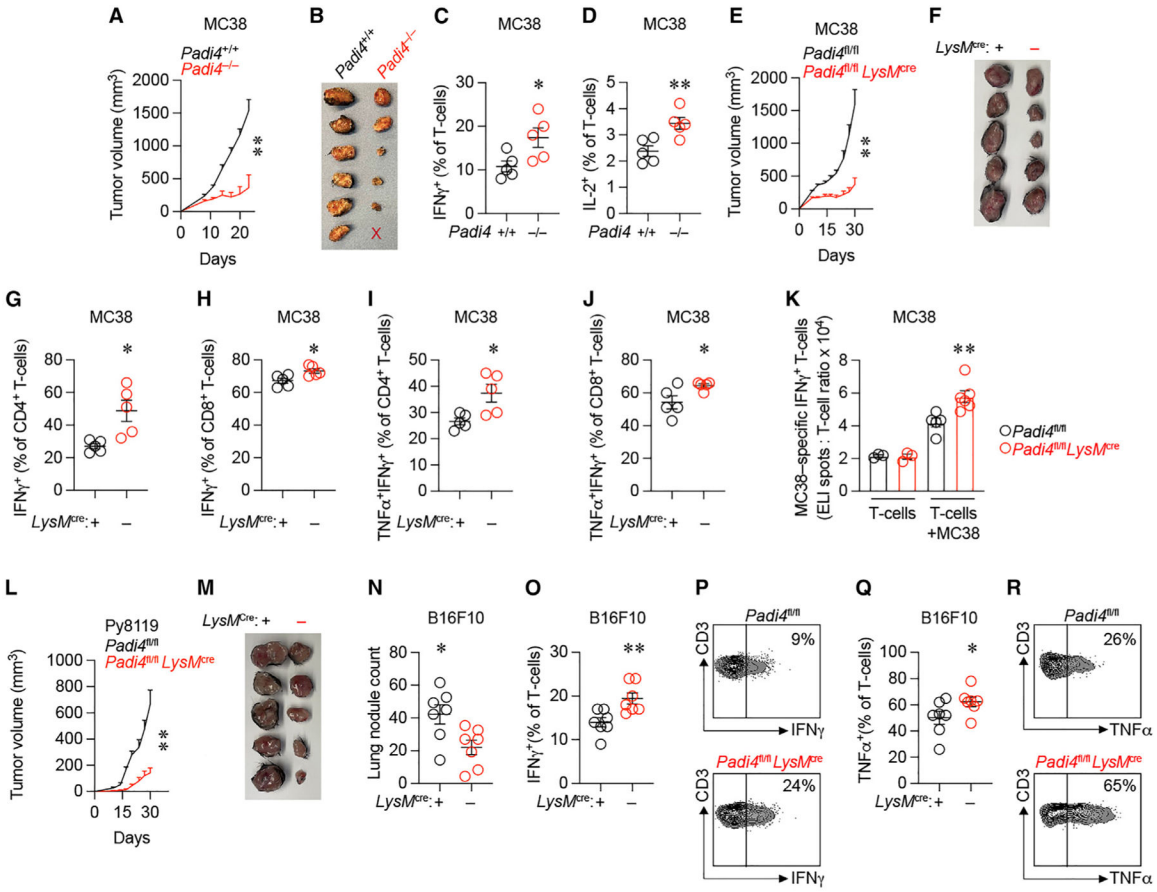

Figure 2. PAD4 in macrophages negatively regulates anti-tumor immunity

(A) Growth kinetics of subcutaneous MC38 murine colorectal cancer in *Padi4*$^{+/+}$ and *Padi4*$^{-/-}$ mice (n = 6).

(B) At endpoint, MC38 tumors from *Padi4*$^{+/+}$ and *Padi4*$^{-/-}$ mice were excised (n = 6).

(C and D) Percentages of IFNγ^+ (C) and IL-2$^+$ (D) T cells from MC38-tumor-bearing *Padi4*$^{+/+}$ and *Padi4*$^{-/-}$ mice (n = 5).

(E) Growth kinetics of subcutaneous MC38 murine colorectal cancer in *Padi4*$^{fl/fl}$ and *Padi4*$^{fl/fl}$ *LysM*^{cre} mice (n = 5).

(F) At endpoint, MC38 tumors from *Padi4*$^{fl/fl}$ and *Padi4*$^{fl/fl}$ *LysM*^{cre} mice were excised (n = 5).

(G and H) Percentages of IFNγ^+CD4$^+$ (G) and IFNγ^+CD8$^+$ (H) T cells from MC38 tumors of *Padi4*$^{fl/fl}$ and *Padi4*$^{fl/fl}$ *LysM*^{cre} mice (n = 5).

(I and J) Percentages of TNFα^+IFNγ^+ CD4$^+$ (I) and TNFα^+IFNγ^+CD8$^+$ (J) T cells from MC38 tumors of *Padi4*$^{fl/fl}$ and *Padi4*$^{fl/fl}$ *LysM*^{cre} mice (n = 5).

(K) Mouse IFNγ enzyme-linked immunosorbent spot (ELISpot) assay measuring IFNγ production in tumor-infiltrating T cells from *Padi4*$^{fl/fl}$ and *Padi4*$^{fl/fl}$ *LysM*^{cre} MC38-bearing mice following stimulation with dead ultraviolet (UV)-irradiated MC38 tumor cells (n = 5–6).

(L) Growth kinetics of subcutaneous Py8119 murine breast cancer in *Padi4*$^{fl/fl}$ and *Padi4*$^{fl/fl}$ *LysM*^{cre} mice (n = 5).

(M) At endpoint, Py8119 tumors from *Padi4*$^{fl/fl}$ and *Padi4*$^{fl/fl}$ *LysM*^{cre} mice were excised (n = 5).

(N) Lung nodule counts on the metastatic lungs excised from *Padi4*$^{fl/fl}$ and *Padi4*$^{fl/fl}$ *LysM*^{cre} mice intravenously inoculated with B16F10 (n = 7).

(O–R) Percentages of IFNγ^+ (O and P) and TNFα^+ (Q and R) tumor-infiltrated T cells from the lung metastasis of B16F10-bearing *Padi4*$^{fl/fl}$ and *Padi4*$^{fl/fl}$ *LysM*^{cre} mice (n = 7).

Data are shown as mean ± SEM (A, C–E, G–L, N, O, and Q). Unpaired two-tailed Student's t test. *$p < 0.05$; **$p < 0.01$.

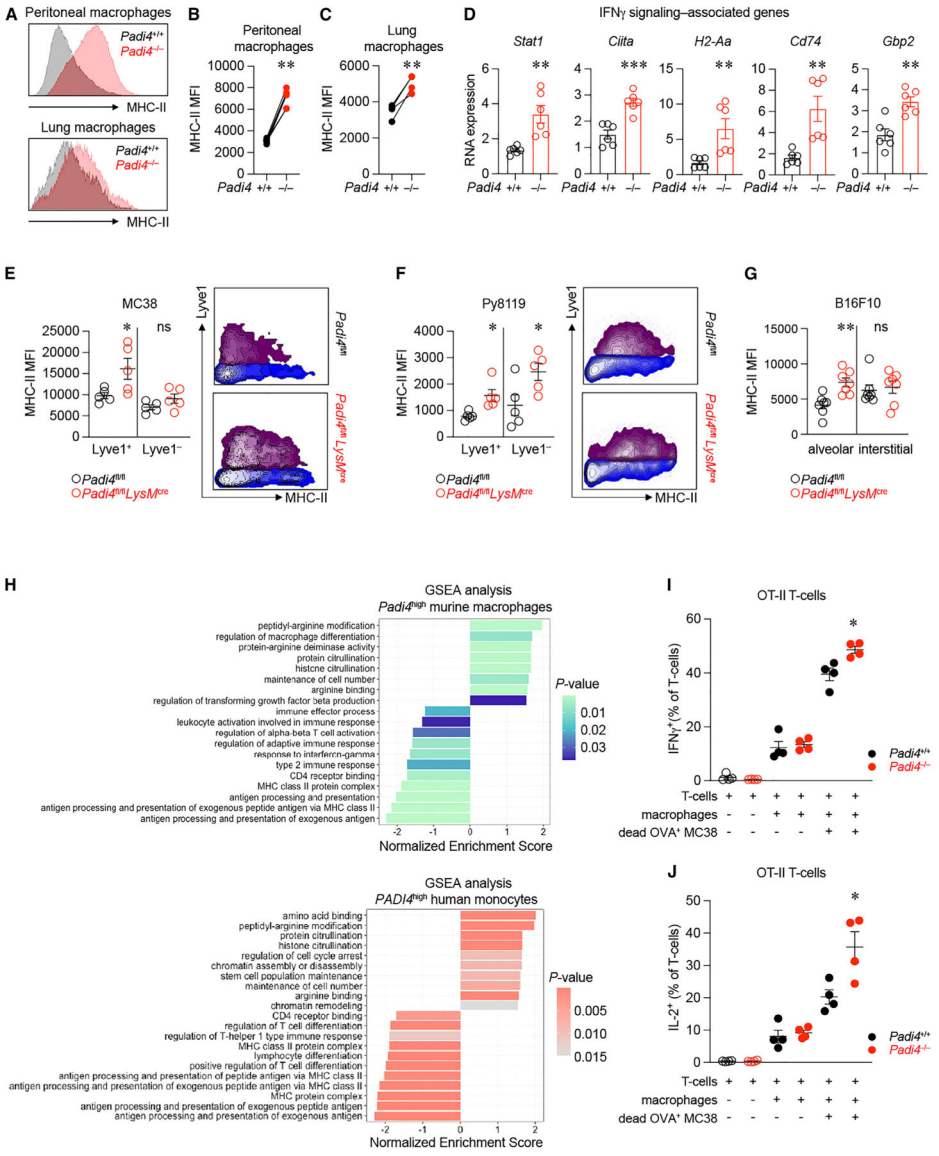

Figure 3. PAD4 restrains MHC class II machinery in macrophages

(A) Representative histogram quantifying MHC class II protein expression in peritoneal and lung macrophages from *Padi4*$^{+/+}$ and *Padi4*$^{-/-}$ mice.

(B) Mean fluorescence intensity (MFI) of MHC class II expression on unchallenged primary peritoneal macrophages harvested from *Padi4*$^{+/+}$ and *Padi4*$^{-/-}$ mice. Representative of nine independent experiments.

(C) MFI of MHC class II expression on unchallenged primary lung macrophages harvested from *Padi4*$^{+/+}$ and *Padi4*$^{-/-}$ mice. Representative of four independent experiments.

(D) Quantitative polymerase chain reaction (qPCR) results showing MHC class II-coding and IFNγ-responsive gene expression in the peritoneal macrophages from healthy *Padi4*$^{+/+}$ vs. *Padi4*$^{-/-}$ mice (n = 6/group, qPCR normalized to β-actin expression).

(E) Fluorescence-activated cell sorting (FACS) analysis showing the MFI of MHC class II in Lyve1^{+} and Lyve1^{-} tumor macrophages from MC38-tumor-bearing *Padi4*$^{fl/fl}$ vs. *Padi4*$^{fl/fl}$ *LysM*^{cre} mice (n = 5).
(F) FACS analysis showing the MFI of MHC class II in Lyve1^{+} and Lyve1^{-} tumor macrophages from Py8119-tumor-bearing *Padi4*$^{fl/fl}$ vs. *Padi4*$^{fl/fl}$ *LysM*^{cre} mice (n = 5).
(G) FACS analysis showing the MFI of MHC class II in alveolar and interstitial lung tumor macrophages from B16F10-bearing *Padi4*$^{fl/fl}$ vs. *Padi4*$^{fl/fl}$ *LysM*^{cre} mice (n = 7).
(H) Gene set enrichment analysis (GSEA) of *Padi4*^{high} mouse peritoneal macrophages from scRNA-seq data of murine peritoneal lavage (GEO: GSE121521) (top). GSEA of *PADI4*^{high} human blood monocytes from scRNA-seq data of human PBMCs (GEO: GSE169246) (bottom).
(I) Percentages of IFNγ^{+} OT-II T cells cultured alone or with *Padi4*$^{+/+}$ or *Padi4*$^{-/-}$ macrophages in the presence or absence of 10^5 UV-irradiated OVA^{+}MC38 cells (n = 4).
(J) Percentages of IL-2^{+} OT-II T cells cultured alone or with *Padi4*$^{+/+}$ or *Padi4*$^{-/-}$ macrophages in the presence or absence of 10^5 UV-irradiated OVA^{+}MC38 cells (n = 4).
Data are shown as mean ± SEM (B–G, I, and J). Unpaired two-tailed Student's t test. *p < 0.05, **p < 0.01, and ***p < 0.001. MFI, mean fluorescence intensity; ns, not significant.

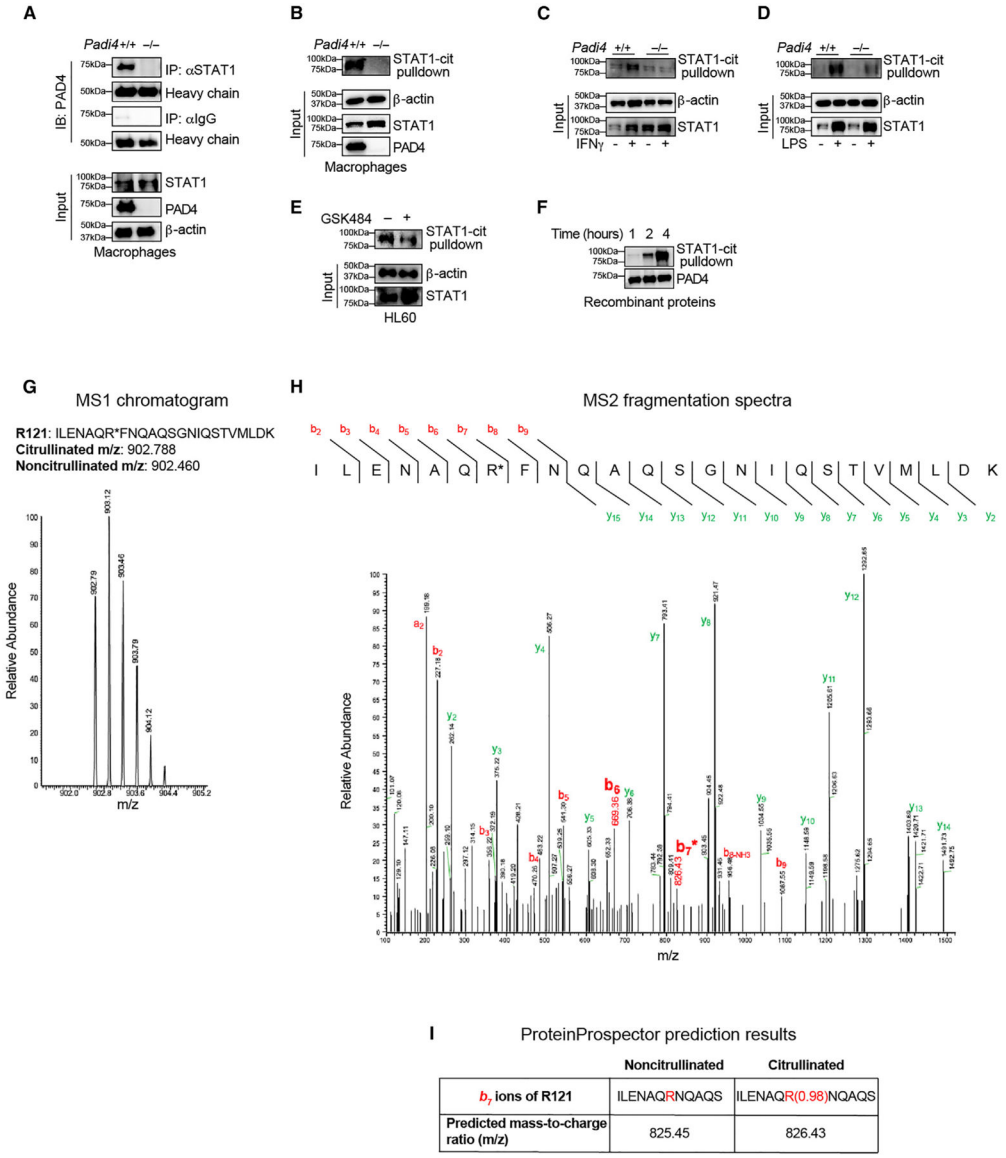

	Noncitrullinated	Citrullinated
b_7 ions of R121	ILENAQRNQAQS	ILENAQR(0.98)NQAQS
Predicted mass-to-charge ratio (m/z)	825.45	826.43

Figure 4. PAD4 citrullinates STAT1 in the N-terminal domain

(A) Tim-4^{+} peritoneal macrophages from *Padi4*$^{+/+}$ and *Padi4*$^{-/-}$ mice were stimulated with 10 ng/mL IFNγ *ex vivo* for 1 h. Whole-cell lysates from *Padi4*$^{+/+}$ vs. *Padi4*$^{-/-}$ Tim-4^{+} macrophages were subjected to immunoprecipitation with anti-STAT1 or control immunoglobulin G (IgG). The immunoprecipitant was probed with anti-PAD4.

(B) *Padi4*$^{+/+}$ and *Padi4*$^{-/-}$ primary mouse Tim-4^{+}-enriched peritoneal macrophages were stimulated with 10 ng/mL IFNγ *ex vivo* for 1 h. STAT1 citrullination was detected via streptavidin pull-down of citrulline-labeled proteins and probed with anti-STAT1.

(C and D) 10 ng/mL IFNγ (C) or 1 μg/mL LPS (D) stimulation of *Padi4*$^{+/+}$ vs. *Padi4*$^{-/-}$ splenocytes for 1 h followed by the detection of citrullinated STAT1.

(E) Treatment of HL60 cells with 10 ng/mL IFNγ and 10 μM GSK484 or DMSO followed by the detection of citrullinated STAT1.

(F) The *in vitro* citrullination assay performed with recombinant human PAD4 (0.5 μg) and recombinant human STAT1 (0.5 μg) proteins supplemented with 2 mM $CaCl_2$ and HEPES.
(G) High-resolution precursor ion (MS1) isotopic envelopes of the R121 peptide of citrullinated STAT1.
(H) MS2 fragmentation spectra originating from the same precursor ion. Observed *b* and *y* ions are indicated. Presence of unmodified b_6 and modified b_7 ions suggests that R121 is citrullinated. The resulting *m/z* of 826.43 due to the modified b_7 ions is indicated in red.
(I) Protein Prospector results revealing the predicted *m/z* at the non-citrullinated vs. citrullinated R121 in the ILENAQRNQAQS peptide. *m/z*, mass-to-charge ratio.

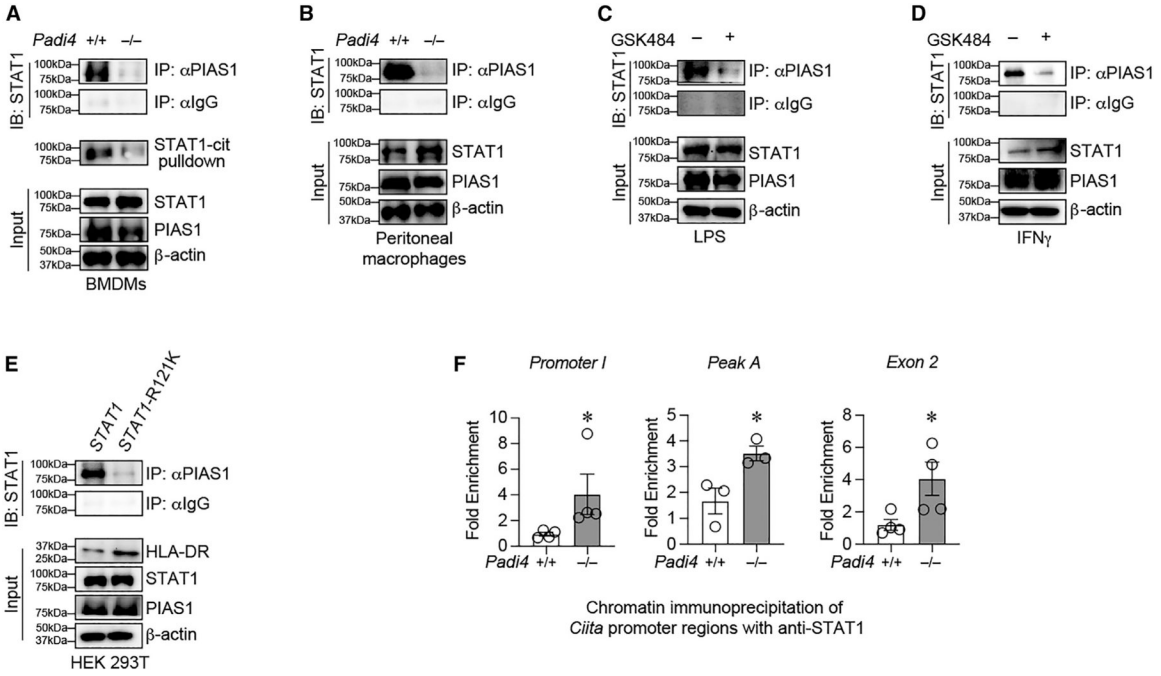

Figure 5. STAT1 citrullination facilitates the STAT1-PIAS1 interaction and MHC class II reduction

(A) *Padi4*$^{+/+}$ and *Padi4*$^{-/-}$ bone marrow-derived macrophages were generated, and proteins were lysed and processed to detect STAT1 citrullination and for the co-immunoprecipitation with anti-PIAS1.

(B) Peritoneal macrophages were harvested from *Padi4*$^{+/+}$ and *Padi4*$^{-/-}$ mice and stimulated with 10 ng/mL IFNγ for 1 h. Proteins were lysed and processed for the co-immunoprecipitation with anti-PIAS1.

(C) HL60 cells were treated with 1 μg/mL LPS for 1 h with or without GSK484, and proteins were lysed and processed for the co-immunoprecipitation with anti-PIAS1.

(D) HL60 cells were treated with 10 ng/mL IFNγ for 1 h with or without GSK484, and proteins were lysed and processed for the co-immunoprecipitation with anti-PIAS1.

(E) A mutant *STAT1* HEK293T cell line in which the R121 was converted into K121 was generated. Cells were treated with 10 ng/mL IFNγ for 1 h, and proteins were lysed and processed to detect HLA-DR levels and for the co-immunoprecipitation with anti-PIAS1.

(F) Chromatin immunoprecipitation was performed on DNA extracted from IFNγ-treated *Padi4*$^{+/+}$ and *Padi4*$^{-/-}$ mouse splenocytes. qPCR primers for the detection of STAT1 at multiple IFNγ-responsive genomic regions in the *CIITA* gene were designed.

Data are shown as mean ± SEM. n = 3–4. One-tailed Mann-Whitney U test. *p < 0.05.

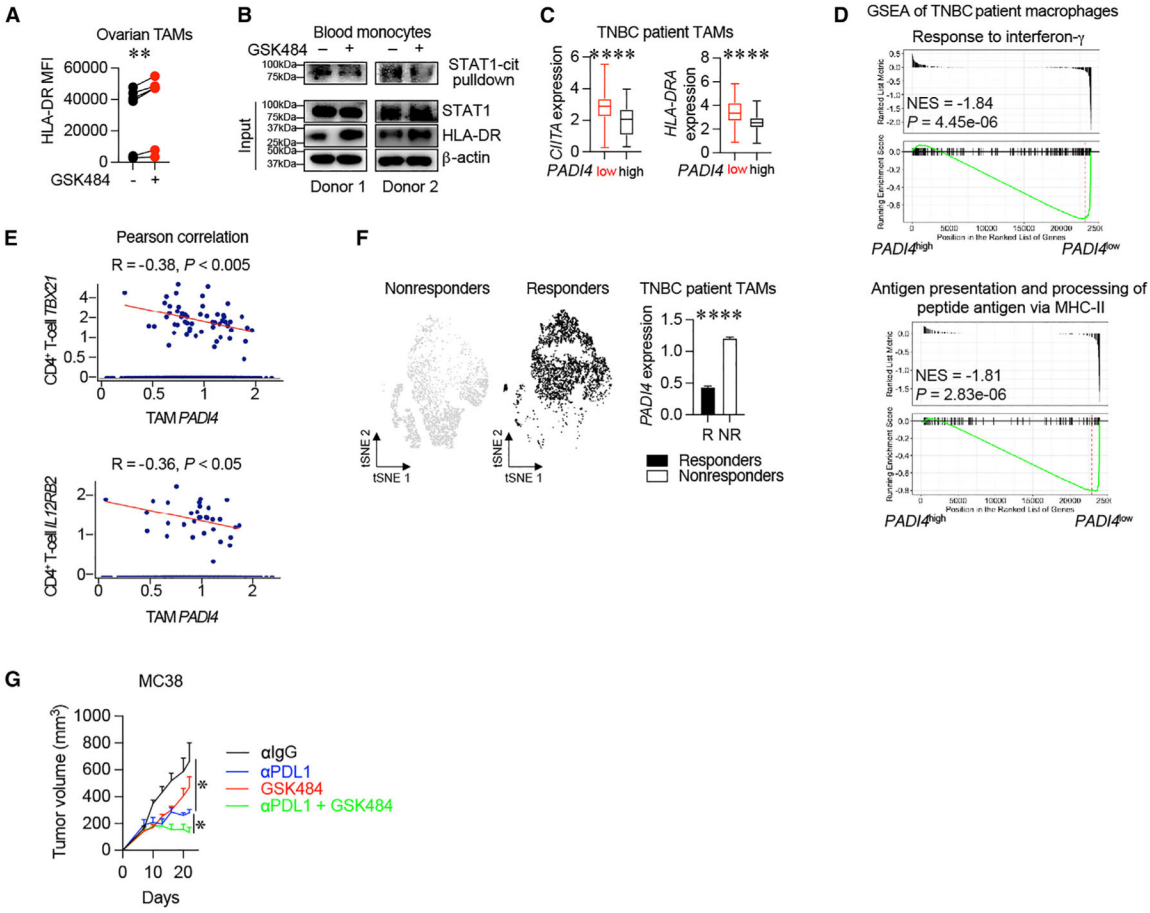

Figure 6. PAD4 negatively correlates with IFNγ signaling and impairs therapeutic response to ICB

(A) Primary human ovarian cancer mononuclear cells were isolated from patient tumors, treated with 10 ng/mL IFNγ and 10 μM GSK484 or DMSO, and then processed to detect $CD45^{+}CD14^{+}$HLA-DR levels via flow cytometry (n = 6).

(B) Primary human macrophages were enriched and derived from PBMCs of blood buffy coats and treated with 10 ng/mL IFNγ and 10 μM GSK484 or DMSO. Proteins were lysed and processed to detect STAT1 citrullination and HLA-DR levels (n = 2).

(C) *CIITA* and *HLA-DRA* expression in PAD4-deficient ($PADI4^{low}$) vs. PAD4-expressing ($PADI4^{high}$) macrophages in patients with TNBC.

(D) GSEA was conducted on $PADI4^{high}$ macrophages, and the normalized enrichment scores (NESs) were assessed for the response to IFNγ and antigen presentation via MHC class II pathways.

(E) Pearson correlations were conducted between TAM *PADI4* expression and the expression effector $CD4^{+}$ T cell genes including *TBX21* and *IL12RB2* in patients with TNBC.

(F) Macrophages were isolated from the total $CD45^{+}$ population of sequenced single cells from patients with TNBC treated with anti-PD-L1 monoclonal antibody (mAb; GEO: GSE169246) (left). $CD33^{+}$ TAMs were further filtered from total responder (R) and non-

responder (NR) macrophages, and *PADI4* expression was assessed between R and NR patients with TNBC (n = 5 responders, n = 6 non-responders) (right).
(G) MC38 tumor progression in wild-type mice treated with or without 4 mg/kg GSK484 or 100 μg anti-PD-L1 mAb treatment (n = 5/group).
Data are shown as mean ± SEM (C, F, and G). Paired two-tailed Student's t test (A). Unpaired two-tailed Student's t test (C, F, and G). *p < 0.05, **p < 0.01, and ****p < 0.0001.

KEY RESOURCES TABLE

REAGENT or RESOURCE	SOURCE	IDENTIFIER
Antibodies		
Rat monocloncal antibody anti-mouse TIM-4 (clone 54)	Cell Signaling Technology	Cat#12-5866-82; RRID: AB_1257163
Rat monocloncal antibody anti-mouse CD90 (clone 30-H12)	BD Bioscience	Cat#553013; RRID: AB_2534246
Rat monocloncal antibody anti-mouse CD4 (clone RM4–5)	BD Bioscience	Cat#553051; RRID: AB_393575
Rat monocloncal antibody anti-mouse CD8 (clone 53–6.7)	BD Bioscience	Cat#564983; RRID: AB_2739032
Rat monocloncal antibody anti-mouse IFNγ (clone XMG1.2)	BD Bioscience	Cat#563773; RRID: AB_2738419
Rat monocloncal antibody anti-mouse IL-2 (clone JES6–5H4)	BD Bioscience	Cat#554429; RRID: AB_398555
Rat monocloncal antibody anti-mouse TNFα (clone MP6-XT22)	BD Bioscience	Cat#557644; RRID: AB_395380
Rat monocloncal antibody anti-mouse CD80 (clone 16–10A1)	BD Bioscience	Cat#563687; RRID: AB_2738376
Rat monocloncal antibody anti-mouse CD86 (clone GL1)	BD Bioscience	Cat#563687; RRID: AB_2738376
Hamster monocloncal antibody anti-mouse CD11c (clone N418)	Invitrogen	Cat# 25-0114-82; RRID: AB_469590
Rat monocloncal antibody anti-mouse CD11b (clone M1/70)	BD Bioscience	Cat# 553312; RRID: AB_398535
Rat monocloncal antibody anti-mouse F4/80 (clone T45–2342)	BD Bioscience	Cat# 565613; RRID: AB_2734770
Mouse monoclonal anti-human Granzyme B (clone GB11)	BD Bioscience	Cat# 561142; RRID: AB_10561690
Rat monoclonal anti-mouse H-2 Class I (clone M1/42)	BD Bioscience	Cat# 566776; RRID: AB_2869859
Rat monoclonal anti-mouse I-A/I-E (clone M5/114.15.2)	BD Bioscience	Cat# 562564; RRID: AB_2716857
Rat monoclonal anti-mouse Ly-6G and Ly-6C (clone RB6–8C5)	BD Bioscience	Cat# 557979; RRID: AB_396971
Mouse monoclonal anti-human CD14 (MØP9)	BD Bioscience	Cat# 562691; RRID: AB_2737725
Mouse monoclonal anti-human CD45 (HI30)	BD Bioscience	Cat# 564106; RRID: AB_2744405
Mouse monoclonal anti-human HLA-DR (L243)	BD Bioscience	Cat# 340688; RRID: AB_627944
Rat anti-mouse LYVE-1 (clone 223322)	Bio-Techne	Cat# FAB2125A; RRID: AB_10972770
7-amino-actinomycin (7AAD)	BD Bioscience	Cat# 51–68981E; RRID: AB_2869265
Recombinant anti-PADI4/PAD4 Rabbit mAb [EPR20706]	Abcam	Cat# ab214810
Anti-MHC Class II Rabbit mAb	Abcam	Cat# ab180779
Anti-HLA-DR Rabbit	Abcam	Cat# ab118347; RRID: AB_10900748
Anti-β-actin (D6A8) mAb	Cell Signaling Technology	Cat# 8457; RRID: AB_10950489
STAT1 Rabbit	Cell Signaling Technology	Cat# 9172; RRID: AB_2198300
Normal Rabbit IgG	Cell Signaling Technology	Cat# 2729; RRID: AB_1031062
PIAS1 (D33A7) XP Rabbit mAb	Cell Signaling Technology	Cat# 3350; RRID: AB_1904090
Goat anti-Rabbit IgG Antibody (H + L), Peroxidase	Vector Laboratories	Cat# PI-1000–1; RRID: AB_2916034
Horse anti-Mouse IgG Antibody (H + L), Peroxidase	Vector Laboratories	Cat# PI-2000–1

REAGENT or RESOURCE	SOURCE	IDENTIFIER
Chemicals, peptides, and recombinant proteins		
Lymphoprep™	STEMCELL	Cat# 7861
Recombinant mouse IFNγ	R&D Systems	Cat# 485-MI
Lipopolysaccharides (LPS) from Escherichia coli O26:B6	Sigma-Aldrich	Cat# L8274
Citrulline-specific Probe-biotin	Cayman Chemical	Cat# 17450
RIPA Lysis Buffer	ThermoFisher	Cat# 89900
IP Lysis Buffer	ThermoFisher	Cat# 87787
Halt Protease Inhibitor Cocktail	ThermoFisher	Cat# 78429
Pierce Streptavidin Agarose	ThermoFisher	Cat# 20353
Protein A/G PLUS-Agarose	Santa Cruz Biotechnology	Cat# sc-2003
GSK484	Sigma-Aldrich	Cat# SML1658
Recombinant human PAD4	Sigma-Aldrich	Cat# SAE0086
Recombinant human STAT1	Abcam	Cat# ab82610
Fast SYBR Green master mix	Abcam	Cat# 4385612
4X Laemmli sample buffer	Bio-Rad	Cat# 161–0747
Ovalbumin	Sigma-Aldrich	Cat# A5503
Trichloroactic acid ACS reagent	Sigma-Aldrich	Cat# T6399
Formaldehyde solution for molecular biology, 36.5–38% in H_2O	Sigma-Aldrich	Cat# F8775
Anti-PE MicroBeads®	Miltenyi Biotec	Cat# 130-048-801
Macrophage Colony stimulating Factor from mouse	Sigma-Aldrich	Cat# M9170
Recombinant human VEGF protein	R&D systems	Cat#293-VE
Recombinant human IL-6 protein	R&D systems	Cat#206-IL
Clarity Western ECL Substrate, 500mL	Bio-Rad	Cat# 1705061
Critical commercial assays		
SimpleChIP® Enzymatic Chromatin IP Kit (Magnetic Beads)	Cell Signaling Technology	Cat# 9003
QuikChange Multi Site-directed Mutagenesis Kit	Agilent	Cat# 200513
EasySep Mouse T cell Isolation Kit	STEMCELL Technologies	Cat# 19851
EasySep Human Monocyte Isolation Kit	STEMCELL Technologies	Cat# 100–0697
LS columns	Miltenyi Biotec	Cat# 130-042-401
Anti-PE Microbeads	Miltenyi Biotec	Cat# 130-048-801
Lipofectamine 2000 Transfection Reagent	Thermo-Fisher	Cat# 11668019
QIAprep Spin Miniprep Kit (50)	QIAGEN	Cat# 27106
ELISpot Plus: Mouse IFN-γ (ALP)	Mabtech	Cat# 3321–4APT-2
Deposited data		
Raw and searched mass spectrometry	This paper	PRIDE: PXD049188
Gene expression profile of patient monocytes and macrophages	(Cassetta et al., 2019)[1]	GEO: GSE117970
Gene expression profile of murine tumor-associated macrophages (TAMs)	(Nixon et al., 2022)[32]	GEO: GSE212643
Gene expression profile of sorted CSF-1R^{high} and CSF-1R^{low} CRC patient TAMs	(Wang et al., 2022)[36]	GEO: GSE193814

REAGENT or RESOURCE	SOURCE	IDENTIFIER
Gene expression profile of sorted Tim-4^{high} and Tim-4^{low} murine peritoneal TAMs	(Xia et al., 2020)[40]	GEO: GSE157673
Gene expression profile of CRC patient immune cells	(Zhang et al., 2020)[34]	GEO: GSE146771
Gene expression profile of healthy mouse peritoneal lavage	(Wang et al., 2020)[33]	GEO: GSE121521
Gene expression profile of human subjects vaccinated with seasonal influenza vaccine	(Wimmers et al., 2021)[49]	GEO: GSE165905
Gene expression profile of *Pias1*$^{+/+}$ and *Pias1*$^{-/-}$ murine BMDMs	(Liu et al.,2004)[66]	GEO: GSE1552
Gene expression profile of TNBC patient immune cells	(Zhang et al., 2021)[35]	GEO: GSE169246
Experimental models: Cell lines		
Mouse cell line: MC38	(Lin et al., 2018)[3]	N/A
Mouse cell line: Py8119	ATCC	Cat# CRL-3278
Mouse cell line: B16F10	ATCC	Cat# CRL-6475
Human cell line: HL60	ATCC	Cat# CCl-240
Human cell line: HEK293T	ATCC	Cat# 3216
Experimental models: Organisms/strains		
Mouse: C57BL/6J	The Jackson Laboratory	Cat# JAX: 000664
Mouse: OT-II TCR transgenic mice	The Jackson Laboratory	Cat# JAX: 004194
Mouse: Padi4-KO (Padi4$^{-/-}$)	Yongqing Li	N/A
Mouse: Padi4 floxed	The Jackson Laboratory	Cat# JAX: 026708
Mouse: LysM cre	The Jackson Laboratory	Cat# JAX: 004781
Mouse: CD4 cre	The Jackson Laboratory	Cat# JAX: 022071
Oligonucleotides		
ChIP-qPCR primers		listed in method details
qPCR primers		listed in method details
Recombinant DNA		
Mutant STAT1-R121K plasmid (h)		listed in method details
STAT1 CRISPR/Cas9 KO Plasmid (h)	Santa Cruz Biotechnology	Cat# sc-400086
Software and algorithms		
Prism 8.0	https://www.graphpad.com/guides/prism/8/user-guide/new-organization.htm	Commercial
Rstudio 3.6.0	https://rstudio.com	Rstudio Team (2020). Rstudio: Integrated Development for R. Rstudio, PBC, Boston, MA
Seurat 4.3.0.1	https://satijalab.org/seurat	Satija et al., 2015[90]
clusterProfiler 3.18.1	https://guangchuangyu.github.io/software/clusterProfiler/	Yu et al., 2012[91]
UMAP 0.2.10.0	https://github.com/lmcinnes/umap	McInnes et al., 2018[92]
Enrichr	https://maayanlab.cloud/Enrichr/	Kuleshov et al., 2016[93]
BART	http://bartweb.org/	Wang et al., 2018[54]
enrichplot	https://github.com/YuLab-SMU/enrichplot	Guangchuang Yu Lab, School of Basic Medical Sciences, Southern Medical University
ggplot2 3.4.2	https://ggplot2.tidyverse.org/	Wickham et al., 2016[94]

REAGENT or RESOURCE	SOURCE	IDENTIFIER
dplyr 1.1.2	https://dplyr.tidyverse.org/news/index.html	Wickham et al., 2023[95]
BD FACSDiva	https://www.bdbiosciences.com/en-us/products/software/instrument-software/bd-facsdiva-software#Overview	BD Bioscience
ProteinProspector v 6.4.9	https://prospector.ucsf.edu/	Baker et al. (1996–2023)[62]